

Bright Planetary Nebulae and their Progenitors in Galaxies Without Star Formation

Michael G. Richer¹

*OAN, Instituto de Astronomía, Universidad Nacional Autónoma de México, P.O. Box 439027, San Diego,
CA 92143*

`richer@astrocen.unam.mx`

and

Marshall L. McCall¹

*Department of Physics & Astronomy, York University, 4700 Keele Street, Toronto, Ontario, Canada M3J
1P3*

`mccall@yorku.ca`

ABSTRACT

We present chemical abundances for planetary nebulae in M32, NGC 185, and NGC 205 based upon spectroscopy obtained at the Canada-France-Hawaii Telescope using the Multi-Object Spectrograph. From these and similar data compiled from the literature for bright planetary nebulae in other Local Group galaxies, we consider the origin and evolution of the stellar progenitors of bright planetary nebulae in galaxies where star formation ceased long ago. The ratio of neon to oxygen abundances in bright planetary nebulae is either identical to that measured in the interstellar medium of star-forming dwarf galaxies or at most changed by a few percent, indicating that neither abundance is significantly altered as a result of the evolution of their stellar progenitors. Several planetary nebulae appear to have dredged up oxygen, but these are the exception, not the rule. The progenitors of bright planetary nebulae typically enhance their original helium abundances by less than 50%. In contrast, nitrogen enhancements can reach factors of 100. However, nitrogen often shows little or no enhancement, without any relation between the level of enrichment and other parameters studied here, suggesting that nitrogen enrichment is a random process. The helium, oxygen, and neon abundances argue that the typical bright planetary nebulae in all of the galaxies considered here are the progeny of stars with initial masses of approximately $1.5 M_{\odot}$ or less, based upon the nucleosynthesis predictions of current theoretical models. These models, however, are unable to explain the nitrogen enrichment or its scatter. Similar conclusions hold for the bright planetary nebulae in galaxies with ongoing star formation. Thus, though composition varies significantly, there is unity in the sense that the progenitors of typical bright planetary nebulae appear to have undergone similar physical processes.

Subject headings: galaxies: abundances—galaxies: individual: M32—galaxies: individual: NGC 185—galaxies: individual: NGC 205—ISM: planetary nebulae (general)—stars: evolution

1. Introduction

The planetary nebula luminosity function (PNLF) has proven remarkably successful as a distance indicator (e.g., Ciardullo et al. 2002).

¹Visiting Astronomer, Canada-France-Hawaii Telescope, operated by the National Research Council of Canada, le Centre National de la Recherche Scientifique de France, and the University of Hawaii

This success is based upon the constancy of the peak luminosity as a function of galaxy morphology, which is presumably a proxy for the mean age of the stellar progenitors of the brightest planetary nebulae (e.g., Marigo et al. 2004). The constancy of the peak luminosity suggests that it is either degenerate to a variety of stellar evolution parameters, or that some subset of planetary nebulae populations are common to the majority of galaxies.

Chemical abundances derived from spectroscopy of the brightest planetary nebulae in different galaxies provide a diagnostic tool to determine how similar these planetary nebulae are. Such studies now exist for many galaxies within the Local Group. Generally, the abundances in bright planetary nebulae trace those in the stellar populations of their host galaxy. Host metallicities span a range of about an order of magnitude, as judged from oxygen abundances in planetary nebulae or from integrated light (see the references in §3 and Table 11). Therefore, bright planetary nebulae do not arise from some stellar population that is common to all or most galaxies, at least as regards chemical composition. These studies can be taken a step further, though, and used to investigate whether the stellar progenitors of these bright planetary nebulae underwent similar evolutionary processes.

It is well-known that the stellar progenitors of planetary nebulae modify their initial chemical composition through the course of their evolution. Furthermore, the chemical abundances that are modified and the extent to which they are modified depend upon the star’s initial mass and metallicity as well as the assumptions adopted concerning convective overshooting, at the lower boundaries of both the convective envelope and the pulse-driven convective zone during a thermal pulse (e.g., Forestini & Charbonnel 1997; Marigo 2001; Herwig 2005; Karakas & Lattanzio 2007). Typically, the matter that is returned to the interstellar medium via the nebular shell is enriched in helium and often in nitrogen, carbon, and s-process elements (e.g., Forestini & Charbonnel 1997; Busso et al. 2001; Marigo 2001). Recently, theoretical work has questioned whether oxygen is also produced (Herwig 2000, e.g.) and some examples where this occurs have been found (e.g., He 2-436 in the Sagittarius dwarf galaxy or the PN

in Sex A; Péquignot et al. 2000; Magrini et al. 2005).

Here, we focus on the general problem of which elemental abundances are modified during the evolution of the progenitors of the brightest planetary nebulae. The brightest planetary nebulae are of greatest interest because they are the ones that are being used to draw inferences about the chemical evolution of their hosts. In particular, we argue that the great majority had progenitors that were not sufficiently massive to dredge up significant quantities of oxygen, which sets an upper limit to their initial mass, or that convective overshooting at the lower boundary of the pulse-driven convective zone is inefficient. Primarily, we focus upon the planetary nebulae in galaxies where star formation ceased long ago, but then also consider the planetary nebulae in galaxies (or galactic components) with ongoing star formation. In Section 2, we present new spectroscopic observations of planetary nebulae in M32, NGC 185, and NGC 205 as well as the reduction and analysis of these data. In Section 3, we compile similar data for the planetary nebulae in other galaxies of the Local Group. In Section 4, we determine what trends exist among elemental abundances and then proceed to interpret these in terms of the evolution of the progenitors of bright planetary nebulae in Section 5. In Section 6, we present our conclusions.

2. Observations and Analysis

2.1. Observations and Data Reductions

The observations were obtained at the Canada-France-Hawaii Telescope using the Multi-Object Spectrograph (MOS; Le Fèvre et al. 1994) on UT 17-19 August 1998. The MOS is a multi-object, imaging, grism spectrograph that uses focal plane masks constructed from previously acquired images. The object slits were chosen to be 1'' wide, but of varying lengths to accommodate the objects of interest. In all cases, however, the slit lengths exceeded 12''. We used a 6001mm⁻¹ grism that gave a dispersion of 105 Å mm⁻¹ and a central wavelength of 4950 Å. The detector was the STIS2 2048 × 2048 CCD. The pixel size was 21 microns, yielding a spatial scale at the detector of 0''.43 pixel⁻¹. The spectral coverage varied depending upon the object’s position within the field of view, but usually covered the 3700-

6700 Å interval. Likewise, the dispersion was typically 2.1 Å pixel^{-1} , but varied depending upon the object’s position within the field of view (from 1.9 Å pixel^{-1} to 2.2 Å pixel^{-1}). Images in the light of $[\text{O III}]\lambda 5007$ and the continuum at 5500Å were acquired on UT 17 August 1998 and used to select objects for observation. Spectra were obtained along columns as detailed in the observing log in Table 1. The photometric calibration was achieved using observations of BD+17°4708, BD+25°3941, BD+26°2606, BD+33°2642, and HD 19445 obtained over the course of the three nights (at least two standard stars were observed per night). Spectra of the mercury, neon, and argon lamps were used to calibrate in wavelength. Pixel-to-pixel variations were removed using spectra of the halogen lamp taken through the masks created for the standard stars and the three galaxies.

The spectra were reduced using the specred package of the Image Reduction and Analysis Facility¹ (IRAF). The procedure for data reduction followed approximately that outlined in Massey et al. (1992). Briefly, the mean of the overscan section was subtracted from all images. A zero-correction image was constructed from overscan-subtracted bias images and was subtracted from all images. The fit1d task was used to fit the columns of the overscan- and zero-correction-subtracted flat field images with a many-piece linear spline to remove the shape of the halogen lamp to form normalized flat field images. Images of the standard stars and the galaxies were divided by the appropriate normalized flat field image. The spectra of the planetary nebulae were then extracted and calibrated in wavelength using the spectra of the arc lamps. Next, the spectra of the standard stars were used to calibrate in flux. Finally, flux- and wavelength-calibrated spectra were co-added to produce the final spectrum for each object.

2.2. Line Intensities

For each planetary nebula, Tables 2-6 present the raw line intensities normalized to $\text{H}\beta$ and their uncertainties (1σ) on a scale where the $\text{H}\beta$ line has

¹IRAF is distributed by the National Optical Astronomical Observatories, which is operated by the Associated Universities for Research in Astronomy, Inc., under contract to the National Science Foundation.

an intensity of 100. The line intensities were measured using the software described in McCall et al (1985). This software simultaneously fits a sampled gaussian profile to the emission line(s) and a straight line to the continuum. The quoted errors include the uncertainties from the fit to the line itself, the fit to the reference line ($\text{H}\beta$), and the noise in the continuum for both lines. For those lines where no uncertainty is quoted, the intensity given is an upper limit (2σ).

Tables 2-6 also include the reddening determined from $\text{H}\alpha/\text{H}\beta$ and $\text{H}\gamma/\text{H}\beta$, assuming intrinsic ratios appropriate for the temperature and density observed. The temperature and density finally adopted for each object is given in Tables 7-9 (see §2.3 for details). Normally, both estimates of the reddening agree within errors, implying that there are no severe errors in the flux calibration. The Fitzpatrick (1999) reddening law was used, parametrized with a total-to-selective extinction of 3.041. This parametrization delivers a true ratio of total-to-selective extinction of 3.07 when integrated over the spectrum of Vega (McCall 2004), which is the average value for the diffuse component of the interstellar medium of the Milky Way (McCall & Armour 2000). The uncertainties quoted for reddenings, temperatures, and densities are derived from the maximum and minimum line ratios allowed considering the uncertainties in the line intensities.

The line intensities were corrected for reddening according to

$$\log \frac{F(\lambda)}{F(\text{H}\beta)} = \log \frac{I(\lambda)}{I(\text{H}\beta)} - 0.4E(B-V)(A_1(\lambda) - A_1(\text{H}\beta)) \quad (1)$$

where $F(\lambda)/F(\text{H}\beta)$ and $I(\lambda)/I(\text{H}\beta)$ are the observed and reddening-corrected line intensity ratios, respectively, $E(B-V)$ is the reddening determined from $F(\text{H}\alpha)/F(\text{H}\beta)$, when available, and $A_1(\lambda)$ is the extinction in magnitudes for $E(B-V) = 1 \text{ mag}$, i.e., $A_1(\lambda) = A(\lambda)/E(B-V)$, $A(\lambda)$ being the reddening law (Fitzpatrick 1999). The values of $A_1(\lambda)$ used for all lines are given in column 3 of Tables 2-6. The optical depth at $1 \mu\text{m}$, which is a much clearer descriptor of the amount of obscuration, can be computed by multiplying $E(B-V)$ by 1.054 (see McCall 2004).

A few of the final spectra of the planetary neb-

ulae in M32 and NGC 205 had anomalously low ratios of $H\alpha/H\beta$. In all cases, these spectra were from slits close to the edges of the field of view (in the spectral direction). The affected spectra are those of PN1 and PN3 in NGC 205 and PN7 and PN30 in M32. These spectra may be identified in Tables 2-6 since a measurement is given for $H\alpha$, but no reddening is computed from the $H\alpha/H\beta$ ratio. In those cases, the line intensity for $H\alpha$ was scaled to the value expected given the reddening found from the $H\gamma/H\beta$ ratio. Also, the line intensities for lines in the red, $\lambda \geq 5876\text{\AA}$, were calculated relative to $H\alpha$ and scaled by the same factor as $H\alpha$. In principle, this effect should be due to some undocumented vignetting within the spectrograph. The principal uncertainty resulting from our correction scheme will be regarding the abundance of He° for the affected objects. N^+ abundances should not be affected due to the proximity of the [N II] lines to $H\alpha$.

All of the planetary nebulae observed here were previously known from the list of Ciardullo et al. (1989), save the object # 3273 from the list of Merrett et al (2006). The finding chart and coordinates for this object are given in Fig. 1.

2.3. Physical Conditions and Chemical Abundances

Tables 7-9 present the electron temperatures as well as the ionic and elemental abundances derived for each object. The atomic data employed for ions of N, O, and Ne are listed in Table 10. For H° and He^+ , the emissivities of Storey & Hummer (1995) were used. For He° , we used an extended list of the emissivities from Porter et al. (2005) that was kindly provided by R. Porter.

The ionic abundances were derived using the SNAP software package (Krawchuk et al. 1997). The electron temperature adopted is always based upon the [O III] $\lambda\lambda 4363/5007$ ratio, the upper limit being used when [O III] $\lambda 4363$ was not detected. An electron density of 2000 cm^{-3} was adopted for all objects, based upon the distribution of densities in Galactic planetary nebulae found by Riesgo & López (2006). When detected, the [S II] $\lambda\lambda 6716, 6731$ lines are usually compatible with this density, within uncertainties. If only an upper limit is available for the lines of a given ion, that limit is used.

Using a lower limit for the electron temperature will underestimate the abundances of oxygen, nitrogen, and neon ions (collisionally-excited lines), while it will slightly overestimate the abundances of helium ions (recombination lines). If limits are available for both an abundance diagnostic and electron temperature, it is not strictly possible to know whether the result is a limit to the ionic abundance. However, since a metal diagnostic varies exponentially with temperature, but linearly with abundance, it is likely that the result is still a lower limit to the ionic abundance.

The elemental abundances were calculated from the ionic abundances using the ionization correction factors (ICFs) proposed by Kingsburgh & Barlow (1994). In this scheme, the N/O and Ne/O abundance ratios that are tabulated in Tables 7-9 are simply the N^+/O^+ and $\text{Ne}^{2+}/\text{O}^{2+}$ ionic ratios, respectively. We are interested primarily in the helium and oxygen abundances and in the N/O and Ne/O abundance ratios, so the ICFs matter most for oxygen. The ICF for oxygen is a function of the He^+ and He^{2+} abundances, and so of the intensities of He I $\lambda 5876$ and He II $\lambda 4686$. We almost always measure He I $\lambda 5876$ (PN30 in M32 is the only exception), but often only have an upper limit to He II $\lambda 4686$. When we only have upper limits to the helium lines, our ICF for oxygen will be slightly overestimated. Nonetheless, since the ICFs are usually near unity (PN30 in M32 is the only exception), any error in the oxygen abundance should also be small. Since the ICFs required to compute the nitrogen and neon abundances are linear functions of the oxygen abundance, any overestimate in the oxygen abundance translates into similar overestimates of the nitrogen and neon abundances, though the N/O and Ne/O ratios are unaffected.

In Tables 7-9, the uncertainties quoted for all quantities account for the uncertainties in the line intensities involved in their derivation, including the uncertainties in the reddening. However, the quoted uncertainties in the elemental abundances do not include the uncertainties in the ICFs.

In the calculation of the elemental abundances, we made an effort to adopt a scheme that treated all objects as homogeneously as possible. Occasionally, this may have resulted in less than optimal elemental abundances for some objects. However, it has the advantage of uniformity, i.e., any

drawbacks are common to all objects. For example, it is feasible to use singlet lines of He I to compute He^+/H in some objects, but not in all. To avoid the risk of introducing spurious differences, we chose to use common lines for all objects. The one exception to this rule is the O^+/H ionic abundance. Generally, the ionic abundance based upon $[\text{O II}]\lambda 3727$ was used in favor of that based upon $[\text{O II}]\lambda\lambda 7319, 7331$, but the latter lines were used when $[\text{O II}]\lambda 3727$ was not available.

2.4. Reliability of the Line Intensities and Elemental Abundances

The uncertainties tabulated for our line intensity measurements are the formal uncertainties associated with the analysis of the data. Given the difficulty of obtaining the data with 4-m-class telescopes, it is helpful to compare with independent measurements of the same objects to gauge the absolute uncertainties. Most valuable to this cause are measurements by Richer & McCall (1995) and Richer et al. (1999). In Fig. 2, we compare our line intensities for planetary nebulae in M32 in common with Richer et al. (1999). Generally, the agreement is reasonable. Lines stronger than $\text{H}\beta$ from both studies agree to within $\pm 10\%$, while lines of order $0.1I(\text{H}\beta)$ have relative uncertainties of $\sim 100\%$. A similar trend is found when comparing the current data for planetary nebulae in NGC 185 and NGC 205 with those presented in Richer & McCall (1995) though fewer data are involved and the measurements of Richer & McCall (1995) are considerably more uncertain than those of Richer et al. (1999). Richer & McCall (2006) discuss this issue further.

Oxygen abundances for some of the planetary nebulae in M32 were previously presented by Richer et al. (1999). We compare the oxygen abundances found here with that study in Fig. 3. Considering that many of the previous abundances were lower limits due the availability of only upper limits for the electron temperatures (i.e., $[\text{O III}]\lambda 4363$ was often not previously detected), we find excellent agreement. In the two cases where there were previously measured temperatures, the oxygen abundance agrees in one case and is apparently discrepant in the other. However, the uncertainties quoted here include the uncertainty in reddening whereas the uncertainties quoted by Richer et al. (1999) do not.

Therefore, this discrepancy is smaller than it appears. Where there were previously temperature limits and now measured temperatures, the current oxygen abundances are higher, as expected. Finally, where there is currently still only a limit to the temperature, the oxygen abundance is higher, again as expected given our better sensitivity (and a lower temperature limit).

3. Data for Planetary Nebulae in Other Galaxies

In order to construct a more representative sample of bright planetary nebulae in galaxies without star formation, we compiled the data available for planetary nebulae in the bulge of M31, M32, NGC 147, Sagittarius, and Fornax from the literature (Walsh et al. 1997; Jacoby & Ciardullo 1999; Richer et al. 1999; Roth et al. 2004; Knaizev et al. 2006; Zijlstra et al. 2006; Gonçalves et al. 2006). For comparison with bright planetary nebulae in galaxies with star formation, we adopt the data compilation from Richer & McCall (2007) augmented with data for planetary nebulae in the disk of M31 from Jacoby & Ford (1986) and Jacoby & Ciardullo (1999) as well as the three planetary nebulae reported here (PN4, PN17, and M3273 in the field of M32). Table 11 summarizes our abundances for the planetary nebulae in all of these galaxies. The total sample consists of 84 and 82 bright planetary nebulae in galaxies with and without star formation, respectively.

The data compiled from the literature were analyzed in the same fashion as described in §2.3 for our own data. One difference, however, is the absence of upper limits to undetected lines of $[\text{O III}]\lambda 4363$ and $\text{He II } \lambda 4686$. When a temperature or its limit could not be determined, no abundances were computed. When $\text{He II } \lambda 4686$ was not detected, the ICF for oxygen is a lower limit (unity), leading to lower limits to the abundances of oxygen, nitrogen, and neon, though N/O and Ne/O are not affected.

We restrict our samples of planetary nebulae to those that are intrinsically brightest, within 2 mag of the brightest in each galaxy. In principle, these should be the objects with the spectra of the highest quality within each galactic sample. We note, however, that all of the planetary nebulae in NGC 147 have intrinsic luminosities considerably

fainter than those included from the other galaxies (Corradi et al. 2005). Selecting objects bright in $[\text{O III}]\lambda 5007$ affects the planetary nebula sample in two known ways (and perhaps in others yet unknown). First, as Fig. 4 illustrates, at least for oxygen abundances below that of the interstellar medium (ISM) in the SMC, high $[\text{O III}]\lambda 5007$ luminosity favors the most oxygen-rich planetary nebulae in each galaxy (Dopita et al. 1992; Richer & McCall 1995), and so may preferentially select objects derived from recent star formation. Second, high $[\text{O III}]\lambda 5007$ luminosity also favors planetary nebulae early in their evolution (e.g., Jacoby 1989; Stasińska et al. 1998; Schönberner et al. 2007).

4. Abundance trends

Figure 5 presents the correlation between neon and oxygen abundances for bright planetary nebulae in different galaxies. To help improve the clarity of this and the following figures, error bars are only shown for the data presented here. For the planetary nebulae in other galaxies, those in dwarf irregulars have somewhat lower uncertainties (especially in the case of Leo A and Sextans A and B), those in Fornax and Sagittarius have much smaller uncertainties, and those in M31 have slightly larger uncertainties. The dashed line shows the Ne-O relation for bright planetary nebulae while the solid line is the relation between these two elements in the interstellar medium in emission-line galaxies (Izotov et al. 2006). A fit of the Ne-O relation for the bright planetary nebulae in galaxies without ongoing star formation (M31 bulge, M32, dwarf spheroidals) yields

$$12 + \log(\text{Ne}/\text{H}) = (1.016 \pm 0.051)X + (-0.87 \pm 0.43), \quad (2)$$

where $X = 12 + \log(\text{O}/\text{H})$. Within uncertainties, this fit is identical to that found by Richer & McCall (2007) for the planetary nebulae in dwarf irregular galaxies. Formally, the slope and intercept differ from the values found by Izotov et al. (2006), but the difference between these relations is minimal, never exceeding 0.05 dex, over the abundance range in common, $7.5 \text{ dex} < 12 + \log(\text{O}/\text{H}) < 8.5 \text{ dex}$.

Figure 6 plots the N/O ratio as a function of oxygen abundance. The solid line is the limit-

ing value of N/O found in star-forming galaxies (Izotov et al. 2006). Although the uncertainties are substantial, since N/O is determined from the N^+/O^+ ratio, both of which are minority species, the scatter does appear to be real. In particular, no anomalously low values are found, suggesting confidence in the N/O ratios.

Figure 7 presents the helium abundance as a function of the oxygen abundance. The solid line is a fit to these elemental abundances in emission-line galaxies from Olive et al. (1997). This relation is a reasonable approximation to a lower envelope for the abundances in planetary nebulae, demonstrating that many planetary nebulae do not modify their original helium content. Note that this relation is only calibrated to $12 + \log(\text{O}/\text{H}) \sim 8.2 \text{ dex}$. Plotting helium abundances as a function of the N/O ratio yields no new information. In particular, no significant correlation is found, though this may be partly due to the large uncertainties in N/O.

In Fig. 8, we attempt to discern cases where oxygen might have been produced by the stellar progenitors by plotting N/Ne versus Ne/O. Planetary nebulae whose progenitors produced oxygen should appear to the left in this diagram. Their vertical position will depend upon whether nitrogen production also took place. We normalize relative to neon since neon is not expected to be modified by the stellar progenitors of most planetary nebulae (Karakas & Lattanzio 2003). Only PN6 and perhaps PN4 in NGC 205 appear to be possible examples of planetary nebulae whose progenitors produced oxygen. From Fig. 5, it would appear that PN56 and FJCHP57 in M31's bulge and disk, respectively, might also have produced oxygen. Unfortunately, neither nitrogen abundances nor uncertainties for the oxygen and neon abundances are available for these two objects.

5. Nucleosynthesis in the Progenitors of Bright Planetary Nebulae

5.1. Oxygen and Neon

On cosmic scales, the production of oxygen and neon is dominated by core collapse supernovae (Clayton 2003; Herwig 2004). Nonetheless, models of the progenitors of planetary nebulae predict that such stars potentially produce both. At very low metallicities, e.g., below one hundredth

of the solar metallicity, the progenitors of planetary nebulae are capable of synthesizing the most abundant isotope of neon, ^{20}Ne (Herwig 2004; Karakas & Lattanzio 2007). At all metallicities, stars with masses in the range $\sim 2-4 M_{\odot}$ produce ^{22}Ne in quantities that can significantly change the observed total neon abundance in planetary nebulae, e.g., change the total abundance by at least +0.1 dex. Finally, depending upon the physics adopted to model semiconvection and convective overshoot in AGB stars, stars with masses of $\sim 2-3 M_{\odot}$ and metallicities comparable to those in the Magellanic Clouds *may* dredge up significant quantities of ^{16}O (our qualitative interpolation of Herwig 2000, 2004). Note that these models achieve significant oxygen dredge-up because of the semi-convection attributed to the pulse-driven convective zone that arises with each helium shell flash and mixes out carbon and oxygen from the outer part of the helium-free core (Herwig 2000). If this convective overshooting is efficient, oxygen is expected to be dredged up along with carbon during the third dredge-up; otherwise no oxygen is dredged up (Marigo 2001; Karakas & Lattanzio 2007). Note that all of these models indicate that oxygen destruction should occur for the progenitors of planetary nebulae with the highest masses. Below $2 M_{\odot}$, current models predict that changes in oxygen and neon abundances should be slight.

Nonetheless, as Karakas & Lattanzio (2003) concluded, the progenitors of planetary nebulae are unlikely to mimic the Ne-O relation found in star-forming galaxies. Any oxygen production in low- or intermediate-mass stars would proceed through the same channel as in high-mass stars, the endpoint of helium burning, via the $^{12}\text{C}(\alpha, \gamma)^{16}\text{O}$ reaction. In high-mass stars, neon is a product of carbon burning (Clayton 2003). In low- or intermediate-mass stars, any ^{22}Ne produced occurs during He-shell burning of CNO-processed material (two alpha captures on ^{14}N , e.g., Herwig 2004) while (at very low metallicities) any ^{20}Ne arises primarily from α particle captures on ^{16}O , $^{16}\text{O}(\alpha, \gamma)^{20}\text{Ne}$ (e.g., Herwig 2004). Thus, while oxygen production will result in the dominant isotope in low- or intermediate-mass stars, most of the neon production would yield a minority isotope. It would therefore be highly coincidental if oxygen and neon production in low- or intermediate-mass stars produced an oxygen-

to-neon ratio identical to that resulting from the nucleosynthesis of high-mass stars.

Figures 5 and 8 argue that oxygen and neon abundances are coupled in the majority of bright planetary nebulae. Since bright planetary nebulae follow the same Ne-O relation as emission line galaxies, where the nucleosynthetic yields of type II supernovae fix the Ne-O relation, the progenitors of bright planetary nebulae either modify both abundances to the same extent or they do not modify either abundance. As we have just argued, the available evidence indicates that the former is highly unlikely. In accord with Karakas & Lattanzio (2003), we conclude that the progenitors of bright planetary nebulae typically do not modify either their oxygen or neon abundances.

Although significant oxygen production is uncommon, both Figs. 5 and 8 indicate that, occasionally, oxygen is produced during the evolution of the stellar progenitors in galaxies where star formation ceased long ago. This conclusion was also reached by Richer & McCall (2007) for the progenitors of bright planetary nebulae in dwarf irregulars, and we extend it here with the example of FJCHP57 in the disk of M31. In general, however, these objects are the exception, not the rule. Note that *all these objects are characterized by unusual Ne/O ratios*.

Based upon luminosity considerations, Ciardullo et al. (2005) have argued that bright planetary nebulae should descend from stars of about $2 M_{\odot}$. (See Richer et al. (1997) for a counter-example.) If bright planetary nebulae do indeed descend from progenitors of about $2 M_{\odot}$, many of the bright planetary nebulae in M32, NGC 185, NGC 205, Fornax, Sagittarius, and the bulge of M31 might be expected to be enriched in oxygen, since many of them have oxygen abundances intermediate between those of the SMC and LMC. These objects, however, have neon and oxygen abundances in accord with the ratio observed in star-forming galaxies, a result that suggests that their oxygen content has not been modified. Therefore, either these bright planetary nebulae descend from progenitors of less massive stars, and hence are less susceptible to oxygen enrichment, or convective overshooting is not as efficient as some models suggest.

Péquignot et al. (2000) have argued in favor of

oxygen production in He 2-436 in Sagittarius, with its progenitor having increased its oxygen content by $7 \pm 4\%$. Such a small increase would not be detectable here, in general, so we cannot rule out production at this level from our abundance measurements. Interestingly, Dudziak et al. (2000) suggest an initial mass of $\sim 1.2 M_{\odot}$ for the progenitor of He 2-436. If this is typical, oxygen production is expected to be slight, regardless of the assumptions concerning convective overshooting (Marigo 2001; Karakas & Lattanzio 2007).

While our individual oxygen and neon abundances are not sufficiently precise to detect small changes in oxygen abundances, the large sample at our disposal should allow us to detect small systematic differences with respect to the neon and oxygen abundances in emission-line galaxies. The slope of our Ne-O relation differs slightly from that found by Izotov et al. (2006) (Fig. 5). Our slope is consistent with unity, as has been found for bright planetary nebulae in dwarf irregular galaxies (Richer & McCall 2007). Izotov et al. (2006) found a slope for the Ne-O relation in star-forming galaxies that is significantly greater than unity. This difference is small, but formally significant, and may be interpreted in a variety of ways.

If neither oxygen nor neon are affected by the evolution of the stellar progenitors and if neither oxygen nor neon production in supernovae changes with metallicity, a slope of unity is expected for the Ne-O relation. Izotov et al. (2006) attributed their larger slope to the depletion of oxygen onto dust grains in H II regions at higher oxygen abundances. However, a slope different from unity might also arise from changes in the reddening law associated with the dust in H II regions or a dependence upon metallicity of the relative production of oxygen and neon in type II supernovae. If the slope found by Izotov et al. (2006) is due to either dust depletion or changes in the reddening law, the slightly shallower slopes found for bright planetary nebulae imply that there is no systematic oxygen production in their progenitors, even in small quantities. If, instead, the slope found by Izotov et al. (2006) reflects the true, changing, production of oxygen and neon by massive stars, the difference between emission-line galaxies and planetary nebulae points to a low level of self-enrichment in the progenitors of bright planetary nebulae proportional to the original oxygen

abundance, of the order of a few percent.

5.2. Helium

Helium abundances span a significant range, even at a given oxygen abundance within a single galaxy (Fig. 7). However, the locus observed for H II regions in star-forming dwarfs (Olive et al. 1997) is a very reasonable fit to the lower boundary of the distribution. Thus it is reasonable to presume that, at a given oxygen abundance, the minimum helium abundance was the initial helium abundance for the progenitors of these planetary nebulae and that the spread in helium abundances is the result of varying enrichments due to the evolution of the progenitors.

We define helium enrichment as the increase in helium abundance observed relative to the helium abundance expected at the same oxygen abundance for dwarf star-forming galaxies (Olive et al. 1997), i.e., fractional enrichment = $((\text{He}/\text{H})_{PN,obs} - (\text{He}/\text{H})_{ISM}) / (\text{He}/\text{H})_{ISM}$. In Fig. 9, we plot histograms of the helium enrichment. We separate bright planetary nebulae into three samples, those in dwarf irregulars, those in dwarf spheroidals and M32, and those in the bulge of M31. The planetary nebulae in the first two samples have oxygen abundances that overlap the range studied by Olive et al. (1997) in the H II regions in star-forming dwarfs.

Clearly, the planetary nebulae in all samples are enriched by less than 50% on average, *if* the relation between oxygen and helium abundances found by Olive et al. (1997) holds. There is a tendency to observe larger helium enrichments in the planetary nebulae in galaxies where star formation ceased long ago, but a Kolmogorov-Smirnov test indicates that the difference between the samples in dwarf irregulars and in M32/dwarf spheroidals is not significant at even the 10% level. Considering theoretically-expected yields (e.g., Marigo 2001), the often low helium enrichments presumably imply that the progenitors of bright planetary nebulae are of rather low mass, probably below $1.5 M_{\odot}$, especially in those systems whose metallicities are below that of the LMC. The bright planetary nebulae in the bulge of M31 appear to imply more enrichment at higher metallicities, but, at these metallicities, the Olive et al. (1997) relation must be extrapolated to compute the enrichment factor (see Fig. 7), so this result is un-

certain.

5.3. Nitrogen

The interpretation of nitrogen is complicated. The history of star formation plays an important role, because nitrogen is produced by both type II supernovae and low- and intermediate-mass stars such as novae and AGB stars, as seen in studies of the ISM in star-forming galaxies (e.g., van Zee et al. 1998). Because of these two nitrogen sources, N/O can vary with time in a complicated way in a galaxy's ISM. For instance, for a constant rate of star formation, the N/O ratio in a galaxy's ISM will initially be fixed at a low value as a result of type II supernovae. As low- and intermediate-mass stars begin to contribute, the N/O ratio will rise, eventually attaining some equilibrium value. For a more complicated star formation rate, the N/O ratio need not vary monotonically with time. Furthermore, the N/O ratio in the ISM is merely the initial value of this ratio in the stellar progenitor of a planetary nebula. If this progenitor star synthesizes nitrogen, the resulting N/O ratio will be even higher. In principle, the N/O ratio is expected to be a function of the mass of the stellar progenitor (e.g., Marigo 2001), so, for a constant star formation rate, one expects a trend of increasing N/O with increasing oxygen abundance in each galaxy.

No such simple result is found. In M32, planetary nebulae spanning a wide range of N/O are found at all oxygen abundances. In the bulge of M31, there are planetary nebulae with similar N/O ratios whose oxygen abundances differ by an order of magnitude. Clearly, then, the N/O ratio is not a monotonic function of the progenitor mass, nor is it solely the result of the chemical evolution of the host galaxy. The scatter of N/O as a function of oxygen abundance is not entirely unexpected (see Fig. 6), as it is seen in bright planetary nebulae in dwarf irregular galaxies (Richer & McCall 2007). Likewise, planetary nebulae in the bulge of the Milky Way span a large range in N/O (Cuisinier et al. 2000; Escudero & Costa 2001; Exter et al. 2004; Górný et al. 2004; Escudero et al. 2004).

In galaxies without star formation, the minimum N/O ratio is similar to the minimum value found in star-forming galaxies up to an oxygen abundance of $12 + \log(\text{O}/\text{H}) \sim 8.5$ dex (data are

limited at higher O/H). A simple interpretation of this result is that the progenitors of their planetary nebulae may have had a similar initial N/O ratio, i.e., the value in the ISM was dominated by the nitrogen production of type II supernovae. If so, the factor by which the progenitor of any planetary nebulae enriched its nitrogen content may be found by comparing the observed N/O ratio with the limiting value in emission line galaxies. This is the maximum enrichment factor, since the progenitor's initial N/O ratio is unknown and could have been higher. Adopting this definition, the progenitors of the planetary nebulae in galaxies without star formation appear to have undergone nitrogen enrichment that varied by more than an order of magnitude. Although the amount of nitrogen enrichment appears to vary randomly, it could conceivably be related to some secondary characteristic of the progenitor stars, such as rotation or binarity.

Since oxygen consumption is not evident in either Figs. 5 or 8, nitrogen production presumably occurs exclusively at the expense of carbon for the bright planetary nebulae in galaxies without ongoing star formation. If the largest nitrogen enrichments occur in progenitors with initial N/O ratios similar to the limiting value in emission line galaxies, the enrichment may be up to a factor of 100. If so, reprocessing of endogenous carbon within the progenitors would be necessary, e.g., via hot bottom burning or some similar process, since the carbon abundance in the interstellar medium is less than 10 times that of nitrogen (Garnett 2002). Such reprocessing of carbon is not predicted in the mass range expected for the progenitors of bright planetary nebulae in systems where star formation stopped long ago.

For $12 + \log(\text{O}/\text{H}) > 8.3$ dex in Fig. 6, the planetary nebulae from galaxies without star formation apparently dominate the lowest values of N/O. If the effect is real, it may result from differences in the chemical evolution of their host galaxies rather than of differences in their stellar progenitors. The higher N/O ratio in planetary nebulae in galaxies with ongoing star formation does not necessarily indicate systematically greater enrichment in these planetary nebulae, since many of these planetary nebulae have N/O ratios compatible with those in the interstellar medium of their host galaxies, i.e., compatible with no en-

richment (Richer & McCall 2007). Therefore, the stellar progenitors in star-forming galaxies need not have produced more nitrogen, but simply may have been born with a higher initial nitrogen content.

5.4. More Generally

A limitation of this entire discussion is our ignorance of the mass range of the progenitors of bright planetary nebulae. In principle, models of nebular luminosities and the expected evolution of the nebular envelopes provide some restrictions, but these are so contradictory as to not be helpful (e.g., Richer et al. 1997; Marigo et al. 2004; Ciardullo et al. 2005; Schönberner et al. 2007). Ideally, the chemical abundances observed in bright planetary nebulae would allow us to constrain the masses of their stellar progenitors.

In galaxies without star formation, planetary nebulae derived from the highest mass progenitors, $M_i > 3 M_\odot$, should be absent. In this case, theory predicts little enrichment in nitrogen (observations of red giants imply enrichment by a factor of up to ~ 4 , e.g., Gratton et al. 2000), and up to a doubling of the helium content. Large enhancements in the oxygen abundance (or none at all) could be common, depending upon the exact masses of the progenitor stars and what physics actually occurs (e.g., Marigo 2001; Karakas & Lattanzio 2007). Likely, changes in neon abundances would be small.

Observations agree with the predictions for helium abundances, though the enhancement is usually less than 50% (Fig. 7). Comparison of oxygen and neon abundances, however, imply that only rarely is oxygen synthesized in quantities exceeding a few percent of the initial abundance. Considering the helium, oxygen, and neon abundances, the bright planetary nebulae in galaxies without star formation are generally consistent with their progenitors having initial masses of about $1.5 M_\odot$ or less, given current theoretical models (e.g., Marigo 2001; Herwig 2005; Karakas & Lattanzio 2007). The main argument against their progenitors having initial masses near $2 M_\odot$ is the rarity of planetary nebulae whose progenitors produced significant quantities of oxygen, unless convective overshoot is inefficient (Marigo 2001; Karakas & Lattanzio 2007). Likewise, the rarity of unusual Ne/O ratios

implies masses below $2 M_\odot$.

The nitrogen abundances in bright planetary nebulae do not agree with the theoretical predictions. Planetary nebulae in galaxies without star formation span a wide range of nitrogen enrichment, from none at all to enrichment exceeding that in red giants by an order of magnitude. The largest nitrogen abundances agree with theoretical expectations only if the progenitors of these planetary nebulae had masses exceeding $3 M_\odot$ (Marigo 2001; Herwig 2005), a possibility excluded by the history of star formation in these galaxies. Even if such masses were allowed, there would remain the problem of very large and very small enrichment at a given progenitor mass (oxygen abundance), e.g., M32 in Fig. 6, since such randomness is not predicted at any mass. Also, if such high masses were invoked to explain the nitrogen abundances, much higher helium abundances should be observed, and they are not.

Fig 8 further emphasizes the difficulty with nitrogen production. All of the objects where oxygen has apparently been dredged up are highly enriched in nitrogen. No models predict significant enrichment in both oxygen and nitrogen simultaneously.

If low mass stars really produce as much nitrogen as these observations suggest, these stars may be a much more important source of this element than has been previously considered. Nitrogen abundances hinge upon the N^+/O^+ ionic ratio. Both ions are minority species in bright planetary nebulae, so the ICF needed to derive the nitrogen abundance is large (see Tables 7-9) and the resulting abundances uncertain. If the nebulae are matter-bounded, the problem would be even more severe. However, the uncertainties for our N/O ratios are driven by uncertainties in line intensities. Typically, the [O II] and [N II] lines are weak and so uncertain, as is also the case for [O III] λ 4363, which is needed to compute the temperatures. Remedying this situation would require deeper spectroscopy. The effort is worthwhile, however, since the low mass progenitors of planetary nebulae represent a substantial fraction of all stellar mass, e.g., the $1 - 1.5 M_\odot$ mass range represents about 16% of the total mass above $1 M_\odot$ for a Salpeter (1955) initial mass function and an upper mass limit of $100 M_\odot$.

Although the foregoing discussion focussed pri-

marily upon the bright planetary nebulae in galaxies where star formation ceased long ago, the bright planetary nebulae in galaxies with ongoing star formation have very similar properties. They too have modest enrichment in helium, negligible enrichment in oxygen, and a wide range of nitrogen enrichments. Therefore, the progenitors of bright planetary nebulae in galaxies with ongoing star formation must also have low masses if current theory is to be trusted.

Thus, chemical abundances argue that the masses of the stellar progenitors of the brightest planetary nebulae are relatively low in all galaxies. This is not necessarily incompatible with the high [O III] λ 5007 luminosities that they achieve, as argued by Richer et al. (1997). In their (somewhat extreme) example of a $0.55M_{\odot}$ central star, 13% of the ionizing radiation need be converted to [O III] λ 5007 photons, which is similar to the maximum efficiency of 10% expected theoretically (Dopita et al. 1992; Marigo et al. 2004). The unknown, as Marigo et al. (2004) make clear, is the lack of quantitative knowledge of the evolution, particularly the time scales, of the planetary nebula system. So, while we may not yet understand why the brightest planetary nebulae descend from these particular progenitor stars, the similarity of these stars from galaxy to galaxy is likely one of the underpinnings of the success of the planetary nebula luminosity function as a distance indicator.

The progenitors of bright extragalactic planetary nebulae span a wide range of chemical compositions, reflecting those of the progenitor stellar populations in their host galaxies. That they enrich the resulting planetary nebulae similarly implies that they underwent similar physical processes during their evolution. Presumably, then, the mass range of these progenitor stars is slightly different from galaxy to galaxy, reflecting the different metallicities of their stellar populations. If so, the epoch of star formation that dominates the production of bright planetary nebulae should vary somewhat from galaxy to galaxy.

Based upon the foregoing, however, it would be a mistake to argue that the masses (or the mass range) of the progenitors of bright planetary nebulae in all galaxies are exactly the same. As shown by Stasińska et al. (1998), the distribution of He II λ 4686/H β intensity ratios is dramatically

different for bright planetary nebulae in the LMC and the bulge of M31. This conclusion appears to hold generally between environments with and without star formation (Richer 2006), implying that the distribution of central star temperatures differs between the two environments. Normally, this is interpreted in terms of the central star mass, but might also result from differences in envelope masses (Stanghellini & Renzini 2000), or both. As argued by both Stasińska et al. (1998) and Richer (2006), it is likely that the ionization structure of the nebulae is also different in environments with and without star formation. Differences in central star masses or in envelope evolution could easily arise from a difference in the mass range of the progenitor stars in different environments.

It would not be unusual if there were surprises lurking regarding the nucleosynthesis in the progenitors of fainter planetary nebulae, especially in galaxies with ongoing star formation. Theory clearly predicts that the planetary nebulae descending from the progenitors of the highest masses should be depleted in oxygen because of hot bottom burning at the base of their convective envelopes (Marigo 2001). Some theoretical work predicts that oxygen production should be common for planetary nebula progenitors with masses of order 2-3 M_{\odot} at metallicities comparable to or lower than the SMC's (Marigo 2001; Herwig 2004). Dwarf irregular galaxies should, therefore, be the typical galactic hosts of planetary nebulae with unusual oxygen abundances. Observationally, however, individual examples are not that common among the brightest planetary nebulae (Richer & McCall 2007), so presumably they are to be found among those of lower [O III] λ 5007 luminosity. The exact luminosities and abundances where oxygen enrichment is common have yet to be identified.

6. Conclusions

We have obtained spectroscopy of a sample of bright planetary nebulae in M32, NGC 185, and NGC 205. From these and similar data for planetary nebulae in other Local Group galaxies, we calculate their chemical composition. These planetary nebulae are generally within 2 mag of the peak of the luminosity function.

We find that helium abundances in bright planetary nebulae are typically changed by less than 50% compared to the initial abundances in their progenitors. Oxygen and neon abundances in bright planetary nebulae are not significantly modified, since they follow the relation between neon and oxygen abundances found in the interstellar medium in star-forming galaxies. There is the possibility of a slight systematic increase in the oxygen abundance by a few percent, but this conclusion depends upon how one interprets the slight variation of the ratio of neon to oxygen as a function of oxygen abundance in star-forming galaxies. In contrast, we often find very strong nitrogen enhancements in bright planetary nebulae, though very small enhancements are also found. These nitrogen enhancements are not obviously related to the progenitor mass or to the chemical evolution of the host galaxy. At present, they appear to be random. In reality, they are likely to be linked to some secondary characteristic of the stellar progenitors, such as rotation or binarity. These conclusions apply independently of whether we consider planetary nebulae in galaxies with or without ongoing star formation.

Considering the helium, oxygen, and neon abundances, bright extragalactic planetary nebulae in all galaxies appear to descend from relatively low mass progenitors, of approximately $1.5 M_{\odot}$ or less, based upon the calibrations of current theoretical models. If their progenitors were significantly more massive, of order $2 M_{\odot}$ as has been argued on the basis of luminosity considerations, significant enrichment in oxygen could be relatively common. A few examples of planetary nebulae with oxygen enrichment are found, but are rare.

The large nitrogen abundances often found suggest more massive stellar progenitors, *i.e.*, exceeding $3 M_{\odot}$ (so as to allow the production of nitrogen via hot bottom burning). Such masses are clearly excluded by the history of star formation in galaxies where star formation stopped long ago, and in any case don't explain the observation of both large and small nitrogen enhancements at a given oxygen abundance. Also, we find no example of a bright extragalactic planetary nebula with very large abundances of both helium and nitrogen, which should be a clear signature of a high mass stellar progenitor. This is the case even for

galaxies where star formation is ongoing. Thus, low- and intermediate-mass stars are a more important source of nitrogen than has been hitherto considered. Despite their difficulty, deeper observations would be very worthwhile to derive more secure abundances.

Overall, the progenitors of all bright extragalactic planetary nebulae appear to have evolved similarly. They were of sufficiently low mass that helium enrichment was modest and oxygen enrichment was minimal, if indeed it even generally takes place. Nevertheless, despite this apparently low mass, these stars produced much greater quantities of nitrogen than are predicted by current models. Presumably, then, the mass range of these stellar progenitors is similar in all galaxies, but displaced somewhat due to metallicity. Consequently, there may be more unity to the properties of bright extragalactic planetary nebulae than has been apparent previously. If this is the case, bright planetary nebulae also presumably probe a particular epoch during the evolution of their host galaxies.

We thank the time allocation committee of the Canada-France-Hawaii Telescope for granting us the opportunity to observe. We thank R. Porter for providing us with a more extensive list of He^o emissivities. MGR acknowledges financial support from CONACyT through grant 43121 and from UNAM-DGAPA via grants IN112103, IN108406-2, and IN108506-2. MLM thanks the Natural Sciences and Engineering Research Council of Canada for its continuing support.

REFERENCES

- Aller, L. H., Keyes, C. D., Maran, S. P., Gull, T. R., Michalitsianos, A. G., & Stecher, T. P. 1987, *ApJ*, 320, 159
- Asplund, M., Grevesse, N., & Sauval, A. J. 2005, in *Cosmic Abundances as Records of Stellar Evolution and Nucleosynthesis*, ASP Conference Series, 336, 25
- Barlow, M. J. 1987, *MNRAS*, 227, 161
- Busso, M., Gallino, R., Lambert, D. L., Travaglio, C., & Smith, V. V. 2001, *ApJ*, 557, 802
- Butler, K. & Zeppen, C. J. 1994, *A&AS*, 108, 1

- Ciardullo, R., Jacoby, G. H., Ford, H. C., & Neill, J. D. 1989, *ApJ*, 339, 53
- Ciardullo, R., Feldmeier, J. J., Jacoby, G. H., Kuzio de Naray, R., Laychak, M. B., & Durrell, P. R. 2002, *ApJ*, 577, 31
- Ciardullo, R., Sigurdsson, S., Feldmeier, J. J., & Jacoby, G. H. 2005, *ApJ*, 629
- Clayton, D. 2003, *Handbook of Isotopes in the Cosmos, Hydrogen to Gallium* (Cambridge, UK: Cambridge University Press)
- Corradi, R. L. M., Magrini, L., Greimel, R., Irwin, M., Leisy, P., Lennon, D. J., Mampaso, A., Perinotto, M. et al. 2005, *A&A*, 431, 555
- Cuisinier, F., Maciel, W. J., Köppen, J., Acker, A., & Stenholm, B. 2000, *A&A*, 353, 543
- Dopita, M. A., Jacoby, G. H., & Vassiliadis, E. 1992, *ApJ*, 389, 27
- Dopita, M. A., & Meatheringham, S. J. 1991, *ApJ*, 367, 115
- Dopita, M. A., Meatheringham, S. J., Webster, B. L., & Ford, H. C. 1988, *ApJ*, 327, 639
- Dudziak, G., Péquignot, D., Zijlstra, A. A., & Walsh, J. R. 2000, *A&A*, 363, 717
- Dufour, R. J., & Talent, D. L. 1980, *ApJ*, 235, 22
- Escudero, A. V., & Costa, R. D. D. 2001, *A&A*, 380, 300
- Escudero, A. V., Costa, R. D. D., & Maciel, W. J. 2004, *A&A*, 414, 211
- Exter, K. M., Barlow, M. J., & Walton, N. A. 2004, *MNRAS*, 349, 1291
- Fitzpatrick, E. L. 1999, *PASP*, 111, 63
- Forestini, M., & Charbonnel, C. 1997, *A&AS*, 123, 241
- Garnett, D. R. 2002, in *Cosmochemistry: The Melting Pot of the Elements. XIII Canary Islands Winter School of Astrophysics*, eds. C. Esteban, R. J. García López, A. Herrero & F. Sánchez (Cambridge, UK: Cambridge University Press), 171
- Gonçalves, D. R., Magrini, L., Leisy, P., & Corradi, R. L. M. 2006, *MNRAS*, in press; also astro-ph/0611756
- Górny, S. K., Stasińska, G., Escudero, A. V., & Costa, R. D. D. 2004, *A&A*, 427, 231
- Gratton, R. G., Sneden, C., Carretta, E., & Bragaglia, A. 2000, *A&A*, 354, 169
- Grevesse, N., & Sauval, A. J. 1998, *Space Science Reviews*, 85, 161
- Henry, R. B. C., Liebert, J., & Boroson, T. A. 1989, *ApJ*, 339, 872
- Herwig, F. 2000, *A&A*, 360, 952
- Herwig, F. 2004, *ApJS*, 155, 651
- Herwig, F. 2005, *ARA&A*, 43, 435
- Hodge, P. W. 1977, *ApJS*, 33, 69
- Hodge, P. W., Kennicutt, R. C., Jr., & Lee, M. G. 1988, *PASP*, 100, 917
- Izotov, Y. I., Stasińska, G., Meynet, G., Guseva, N. G., & Thuan, T. X. 2006, *A&A*, 448, 955
- Jacoby, G. H., & Ciardullo, R. 1999, *ApJ*, 515, 169
- Jacoby, G. H. 1989, *ApJ*, 339, 39
- Jacoby, G. H., & Ford, H. C. 1986, *ApJ*, 304, 490
- Jacoby, G. H., & Kaler, J. B. 1993, *ApJ*, 417, 209
- Karakas, A., & Lattanzio, J. C. 2003, *PASA*, 20, 393
- Karakas, A., & Lattanzio, J. C. 2007, astro-ph/0708.4385
- Kauffman, V. & Sugar, S. 1986, *JPCRD*, 15, 332
- Killen, R. M., & Dufour, R. J. 1982, *PASP*, 94, 444
- Kingsburgh, R. L., & Barlow, M. J. 1994, *MNRAS*, 271, 257
- Kniazev, A. Y., Grebel, E. K., Pustilnik, S. A., & Pramskij, A. G. 2006, *A&A*, submitted
- Kniazev, A. Y., Grebel, E. K., Pustilnik, S. A., Pramskil, A. G., & Zucker, D. B. 2005, *AJ*, 130, 1558

- Krawchuk, C., McCall, M. L., Komljenovic, M., Kingsburgh, R., Richer, M., Stevenson, C. 1997, in IAU Symp. 180, Planetary Nebulae, ed. H. J. Habing & H. J. G. L. M. Lamers (Dordrecht: Kluwer), 116,
- Le Fèvre, O., Crampton, D., Felenbock, P., & Monnet, G. 1994, *A&A*, 282, 325
- Lee, H., McCall, M. L., Kingsburgh, R. L., Ross, R., & Stevenson, C. 2003, *AJ*, 125, 146
- Lee, H., Skillman, E. D., & Venn, K. A. 2006, personal communication
- Leisy, P., Corradi, R. L. M., Magrini, L., Greimel, R., Mampaso, A., & Dennefeld, M. 2005a, *A&A*, 436, 437
- Leisy, P., & Dennefeld, M. 1996, *A&AS*, 116, 95
- Leisy, P., Magrini, L., Corradi, R. L. M., & Mampaso, A. 2005b, in Planetary Nebulae as Astronomical Tools, eds. R. Szczerba, G. Stasińska, & S. Górny (AIP: Melville, USA), 265
- Leisy, P., Magrini, L., Corradi, R. L. M., & Mampaso, A. 2006, in Planetary Nebulae Beyond the Milky Way, eds. L. Stanghellini, J. R. Walsh, and N. G. Douglas (Springer: Berlin, Germany), 252
- Lennon, D. J. & Burke, V. M. 1994, *A&AS*, 103, 273
- Magrini, L., Leisy, P., Corradi, R. L. M., Perinotto, M., Mampaso, A., & Vílchez, J. M. 2005, *A&A*, 443, 115
- Marigo, P. 2001, *A&A*, 370, 194
- Marigo, P., Girardi, L., Weiss, A., Groenewegen, M. A. T., & Chiosi, C. 2004, *A&A*, 423, 995
- Massey, P., Valdes, F., & Barnes, J. 1992, *A User's Guide to Reducing Slit Spectra with IRAF*, IRAF User Guide, Vol. 2B (Tucson: National Optical Astronomy Observatory)
- Mateo, M. 1998, *ARA&A*, 36, 435
- McCall, M. L. 2004, *AJ*, 128, 2144
- McCall, M. L., Rybski, P. M., & Shields, G. A. 1985, *ApJS*, 57, 1
- McCall, M. L., & Armour, M.-H. 2000, in Mapping the Hidden Universe: The Universe Behind the Milky Way - The Universe in H I, ASP Conf. Ser., eds. R. C. Kraan-Korteweg, P. A. Henning, & H. Andernach (San Francisco: Astronomical Society of the Pacific), 218, 1
- McLaughlin, B. M., & Bell, K. L. 1993, *ApJ*, 408, 753
- Meatheringham, S. J., & Dopita, M. A. 1991a, *ApJS*, 76, 1085
- Meatheringham, S. J., & Dopita, M. A. 1991b, *ApJS*, 75, 407
- Meatheringham, S. J., Dopita, M. A., & Morgan, D. H. 1988, *ApJ*, 329, 166
- Méndez, R. H., Thomas, D., Saglia, R. P., Maraston, C., Kudritzki, R. P., & Bender, R. 2005, *ApJ*, 627, 767
- Mendoza, C., & Zeppen, C. J. 1982, preliminary result quoted in Mendoza, C. 1983, in Planetary Nebulae (IAU Symp. 103), ed. D. R. Flower (D. Reidel Publishing Co.: Dordrecht, Holland), 143
- Merrett, H. R., Merrifield, M. R., Douglas, N. G., Kuijken, K., Romanowsky, A. J., Napolitano, N. R., Arnaboldi, M., Capaccioli, M., Freeman, K. C., Gerhard, O., Coccato, L., Carter, D., Evans, N. W., Wilkinson, M. I., Halliday, C., & Bridges, T. J. 2006, *MNRAS*, 369, 120
- Monk, D. J., Barlow, M. J., & Clegg, R. E. S. 1987, *MNRAS*, 234, 583
- Olive, K. A., Steigman, G., & Skillman, E. D. 1997, *ApJ*, 483, 788
- Pagel, B. E. J., Edmunds, M. G., & Smith, G. 1980, *MNRAS*, 192, 219
- Peimbert, A., Peimbert, M., & Ruíz, M. T. 2005, *ApJ*, 634, 1056
- Peña, M., Richer, M. G., & Stasińska, G. 2006, in Planetary Nebulae in our Galaxy and Beyond (IAU Symp. 234), eds. M. J. Barlow and R. H. Méndez (Cambridge U. Press: Cambridge, UK), in press
- Péquignot, D., Walsh, J. R., Zijlstra, A. A., & Dudziak, G. 2000, *A&A*, 361, L1

- Porter, R. L., Bauman, R. P., Ferland, G. J., & MacAdam, K. B. 2005, *ApJL*, 622, 73
- Pradhan, A. K. 1976, *MNRAS*, 177, 31
- Richer, M. G. 1993, *ApJ*, 415, 240
- Richer, M. G. 2006, in *Planetary Nebulae in our Galaxy and Beyond (IAU Symp. 234)*, eds. M. J. Barlow and R. H. Méndez (Cambridge U. Press: Cambridge, UK), 317; also astro-ph/0605348
- Richer, M. G., & McCall, M. L. 1995, *ApJ*, 445, 642
- Richer, M. G., & McCall, M. L. 2006, *Planetary Nebulae Beyond the Milky Way, ESO Astrophysics Symposia*, eds. L. Stanghellini, J. R. Walsh, and N. G. Douglas (Springer Verlag: Berlin), 220; also astro-ph/0407327
- Richer, M. G., & McCall, M. L. 2006, *ApJ*, 658, 328
- Richer, M. G., McCall, M. L., & Arimoto, N. 1997, *A&AS*, 122, 215
- Richer, M. G., Stasińska, G., & McCall, M. L. 1999, *A&AS*, 135, 203
- Riesgo, H., & López, J. A. 2006, *RMAA*, 42, 47
- Roth, M. M., Becker, T., Kelz, A., & Schmoll, J. 2004, *ApJ*, 603, 531
- Russell, S. C., & Dopita, M. A. 1992, *ApJ*, 384, 508
- Salpeter, E. E. 1955, 121, 161
- Schönberner, D., Jacob, R., Steffen, M., & Sandin, C. 2007, *A&A*, 473, 467
- Schlattl, H., Salaris, M., Cassisi, S., & Weiss, A. 2002, *A&A*, 395, 77
- Siess, L., Livio, M., & Lattanzio, J. 2002, *ApJ*, 570, 329
- Stanghellini, L., & Renzini, A. 2000, *ApJ*, 542, 308
- Stasińska, G., Richer, M. G., & McCall, M. L. 1988, *A&A*, 336, 667
- Storey, P. J., & Hummer, D. G. 1995, *MNRAS*, 272, 41
- van Zee, L., Salzer, J. J., & Haynes, M. P. 1998, *ApJL*, 497, 1
- van Zee, L., Skillman, E. D., & Haynes, M. P. 2006, *ApJ*, 637, 269
- Vassiliadis, E., Dopita, M. A., Morgan, D. H., & Bell, J. F. 1992, *ApJS*, 83, 87
- Walsh, J. R., Dudziak, G., Minniti, D., & Zijlstra, A. A. 1997, *ApJ*, 487, 651
- Walsh, J. R., Walton, N. A., Jacoby, G. H., & Peletier, R. F. 1999, *A&A*, 346, 753
- Wiese, W. L., Fuhr, J. R. & Deters, T. M. 1996, *JPCRD*, Monograph 7
- Wood, P. R., Meatheringham, S. J., Dopita, M. A., & Morgan, D. H. 1987, *ApJ*, 320, 178
- Zijlstra, A. A., Gesicki, K., Walsh, J. R., Péquignot, D., van Hoof, P. A. M., & Minniti, D. 2006, *MNRAS*, submitted, also astro-ph/0603422

This 2-column preprint was prepared with the AAS L^AT_EX macros v5.2.

TABLE 1
SPECTROSCOPY OBSERVING LOG

Date (UT)	Galaxy	Exposures
17 Aug 1998	NGC 205	5 × 1800s
18 Aug 1998	NGC 185	5 × 1800s
	NGC 205	3 × 1800s
19 Aug 1998	M32	7 × 1800s
	NGC 185	2 × 1800s

TABLE 2
OBSERVED LINE INTENSITIES^a FOR PNE IN NGC 185

Wavelength	Ion	$A_1(\lambda)^b$	PN3	PN5	PN1	PN2	PN4
3727	[O II]	4.52	22 ± 13	< 19	9.7 ± 2.4	32.9 ± 7.1	< 65
3868.76	[Ne III]	4.39	84 ± 12	36 ± 8	71.0 ± 2.6	30.6 ± 3.1	57 ± 16
3889.049	H I	4.37		17.0 ± 6.7	12.7 ± 2.1	13.6 ± 2.6	
3967.47	[Ne III]	4.30	46 ± 11	16.8 ± 7.4	27.1 ± 2.7	6.8 ± 3.1	
3970.072	H I	4.29		18.0 ± 7.5	11.0 ± 2.6	11.9 ± 3.2	
4101.765	H I	4.18		21.3 ± 5.0	18.7 ± 1.4	17.6 ± 2.1	21 ± 9
4340.495	H I	3.97	38.7 ± 4.8	42.0 ± 4.8	41.7 ± 1.1	41.7 ± 1.6	41.4 ± 6.8
4363.21	[O III]	3.95	26.6 ± 4.4	18.9 ± 4.1	24.5 ± 1.0	3.3 ± 1.1	20.9 ± 5.6
4471.477	He I	3.86			5.36 ± 0.89	6.1 ± 1.2	
4685.75	He II	3.66	43.0 ± 4.6	13.3 ± 3.7	8.94 ± 0.79	< 2	< 11
4861.332	H I	3.49	100.0 ± 3.8	100.0 ± 4.2	100.00 ± 0.85	100.0 ± 1.3	100.0 ± 7.4
4958.92	[O III]	3.39	582 ± 17	296.3 ± 9.9	368.9 ± 2.7	231.3 ± 2.6	397 ± 22
5006.85	[O III]	3.34	1776 ± 50	902 ± 27	1112.1 ± 6.8	701.5 ± 6.5	1173 ± 63
5875.666	He I	2.65	14.1 ± 2.5	17.7 ± 3.5	22.37 ± 0.81	18.07 ± 1.14	17.9 ± 4.7
6300.32	[O I]	2.40	54.0 ± 5.0		9.25 ± 0.77	10.0 ± 1.2	
6312.06	[S III]	2.39			2.72 ± 0.63	2.71 ± 0.98	
6363.81	[O I]	2.36	18.7 ± 4.1		2.35 ± 0.63	4.44 ± 1.07	
6548.06	[N II]	2.26	76.7 ± 4.8	12.8 ± 3.7	10.8 ± 1.6	14.6 ± 1.6	
6562.817	H I	2.26	496 ± 15	353 ± 12	387.1 ± 3.1	351.7 ± 3.7	348 ± 20
6583.39	[N II]	2.25	224.2 ± 7.8	23.6 ± 4.0	31.9 ± 1.7	44.8 ± 1.7	< 8
6678.149	He I	2.20	5.0 ± 2.9	< 6	5.00 ± 0.66	6.38 ± 1.24	
6716.42	[S II]	2.18	5.5 ± 2.8	< 6	2.10 ± 0.56	3.50 ± 1.10	< 8
6730.78	[S II]	2.17	19.8 ± 3.8	< 6	2.97 ± 0.61	6.4 ± 1.3	< 8
7065.188	He I	2.01			17.34 ± 0.90	12.37 ± 1.21	
7135.8	[Ar III]	1.98	35.3 ± 4.1		11.00 ± 0.83	13.72 ± 1.23	
7319.92	[O II]	1.90			7.89 ± 1.22		
7330.19	[O II]	1.90			4.08 ± 1.02		
$E(B - V)_{H\alpha}$	(mag)		0.51 ± 0.03	0.21 ± 0.04	0.30 ± 0.01	0.18 ± 0.02	0.20 ± 0.06
$E(B - V)_{H\gamma}$	(mag)		0.45 ± 0.28	0.27 ± 0.26	0.29 ± 0.06	0.26 ± 0.09	0.30 ± 0.38

^aThe scale is such that $F(H\beta) = 100$. If no uncertainty is quoted, the value is a 2σ upper limit to the line intensity.

^b $A_1(\lambda)$ is the extinction for a reddening $E(B - V) = 1$ mag, derived from the Fitzpatrick (1999) reddening law parametrized with a ratio of total-to-selective extinction of 3.041.

TABLE 3
OBSERVED LINE INTENSITIES^a FOR PNE IN NGC 205

Wavelength	Ion	$A_1(\lambda)^b$	PN2	PN3	PN26	PN10	PN1	PN9	PN8	PN7
3727	[O II]	4.52	103 ± 38	17.9 ± 8.3	< 30		43 ± 14	< 82	< 38	< 17
3868.76	[Ne III]	4.39	< 50		< 30		23.4 ± 6.7	59 ± 19		26.0 ± 5.0
3889.049	H I	4.37								5.9 ± 3.9
3967.47	[Ne III]	4.30	< 50							15.2 ± 5.4
3970.072	H I	4.29		18.0 ± 4.3			22.4 ± 5.8			16.9 ± 5.4
4101.765	H I	4.18		15.5 ± 2.8	25.6 ± 9.9		20.5 ± 5.2			13.5 ± 2.8
4340.495	H I	3.97	34 ± 12	32.9 ± 3.3	37.4 ± 6.8	32 ± 10	35.4 ± 3.3	36 ± 10	37.3 ± 7.1	37.0 ± 2.6
4363.21	[O III]	3.95	< 23	4.6 ± 2.4	< 11	< 18	4.7 ± 2.2	< 14	24.2 ± 5.8	8.5 ± 2.0
4471.477	He I	3.86		5.2 ± 2.4			9.7 ± 2.6			3.5 ± 1.8
4685.75	He II	3.66	< 5	< 3	< 8	< 17	3.3 ± 1.8	< 12	7.5 ± 4.4	< 3
4861.332	H I	3.49	100.0 ± 8.2	100.0 ± 2.7	100.0 ± 6.9	100.0 ± 7.4	100.0 ± 3.1	100.0 ± 6.9	100.0 ± 6.9	100.0 ± 2.5
4958.92	[O III]	3.39	433 ± 28	161.0 ± 4.2	204 ± 12	387 ± 24	221.9 ± 5.9	360 ± 21	394 ± 22	335.5 ± 7.9
5006.85	[O III]	3.34	1354 ± 83	483.9 ± 9.8	661 ± 36	1217 ± 71	674 ± 15	1092 ± 58	1221 ± 67	1025 ± 19
5875.666	He I	2.65	32.9 ± 6.3	43.6 ± 5.2	25.1 ± 4.7	25.6 ± 7.3	31.2 ± 4.1	27.2 ± 6.0	25.6 ± 4.2	26.3 ± 1.9
6300.32	[O I]	2.40	23.6 ± 5.5							
6548.06	[N II]	2.26		21.4 ± 5.0	22.4 ± 4.6	25.6 ± 7.2	32.3 ± 4.4	22.6 ± 7.3	11.9 ± 4.4	10.8 ± 3.3
6562.817	H I	2.26	459 ± 30	700 ± 15	548 ± 30	593 ± 36	578 ± 14	675 ± 36	533 ± 30	495.8 ± 9.9
6583.39	[N II]	2.25	8.4 ± 7.0	54.0 ± 5.4	54.3 ± 5.5	69.5 ± 8.7	59.9 ± 4.7	73.6 ± 8.8	17.8 ± 4.7	34.5 ± 3.5
6678.149	He I	2.20		14.7 ± 3.4	8.2 ± 3.2	17.7 ± 5.6				8.0 ± 1.6
6716.42	[S II]	2.18	< 14	< 6	< 5	< 9	< 7	< 10	< 6	2.6 ± 1.3
6730.78	[S II]	2.17	< 14	< 6	< 5	< 9	< 7	< 10	< 6	6.1 ± 1.4
7065.188	He I	2.01			21.6 ± 5.7	26.9 ± 6.5		36.8 ± 8.3		17.1 ± 1.9
7135.8	[Ar III]	1.98	28.7 ± 6.9		29.4 ± 6.1	31.0 ± 5.9		50.8 ± 9.0	25.0 ± 4.2	20.8 ± 2.0
7319.92	[O II]	1.90			16.3 ± 5.4			< 15		10.8 ± 2.5
7330.19	[O II]	1.90			12.2 ± 5.1			< 15		4.0 ± 1.8
$E(B - V)_{H\alpha}$	(mag)		0.45 ± 0.06		0.60 ± 0.05	0.67 ± 0.06		0.78 ± 0.05	0.58 ± 0.06	0.50 ± 0.02
$E(B - V)_{H\gamma}$	(mag)		0.72 ± 0.82	0.81 ± 0.24	0.53 ± 0.41	0.89 ± 0.75	0.63 ± 0.22	0.64 ± 0.66	0.54 ± 0.44	0.54 ± 0.16

^aThe scale is such that $F(H\beta) = 100$. If no uncertainty is quoted, the value is a 2σ upper limit to the line intensity.

^b $A_1(\lambda)$ is the extinction for a reddening $E(B - V) = 1$ mag, derived from the Fitzpatrick (1999) reddening law parametrized with a ratio of total-to-selective extinction of 3.041.

TABLE 4
OBSERVED LINE INTENSITIES^a FOR PNE IN NGC 205 (CONT.)

Wavelength	Ion	$A_1(\lambda)^b$	PN6	PN5	PN4	PN24	PN19
3727	[O II]	4.52		20.9 ± 5.6	15.0 ± 6.6	130 ± 15	< 111
3868.76	[Ne III]	4.39	21.4 ± 6.8	50.2 ± 4.2	35.9 ± 7.2		
3889.049	H I	4.37		7.1 ± 3.3	10.8 ± 5.6		
3967.47	[Ne III]	4.30		22.1 ± 4.3	18.1 ± 6.9		
3970.072	H I	4.29	24.8 ± 5.8	5.8 ± 4.0	11.5 ± 6.2		
4101.765	H I	4.18	18.5 ± 3.7	17.5 ± 3.3	16.3 ± 3.4	31.8 ± 5.3	
4340.495	H I	3.97	38.8 ± 3.4	38.8 ± 1.9	37.4 ± 3.1	48.8 ± 3.8	33.9 ± 7.5
4363.21	[O III]	3.95	20.5 ± 3.0	10.2 ± 1.6	20.2 ± 2.8	< 6	49.8 ± 8.6
4471.477	He I	3.86		3.4 ± 1.4	5.8 ± 2.4	7.8 ± 2.7	
4685.75	He II	3.66	25.2 ± 2.4	5.8 ± 1.4	11.5 ± 1.8	< 3±	28.5 ± 7.8
4861.332	H I	3.49	100.0 ± 3.4	100.0 ± 1.4	100.0 ± 1.9	100.0 ± 3.0	100.0 ± 8.9
4958.92	[O III]	3.39	473 ± 13	455.7 ± 5.0	410.1 ± 6.4	88.6 ± 4.5	137 ± 11
5006.85	[O III]	3.34	1443 ± 36	1373.8 ± 14	1251 ± 17	264.4 ± 7.3	430 ± 28
5875.666	He I	2.65	14.6 ± 2.0	17.9 ± 1.1	24.2 ± 1.9	10.6 ± 1.8	< 13
6300.32	[O I]	2.40	15.5 ± 2.3	14.0 ± 1.4			
6312.06	[S III]	2.39	5.3 ± 1.8	3.8 ± 1.1			
6363.81	[O I]	2.36	6.8 ± 1.8	5.7 ± 1.2			
6548.06	[N II]	2.26	28.0 ± 3.8	19.2 ± 3.8	17.7 ± 3.6		10.6 ± 5.1
6562.817	H I	2.26	450 ± 12	423.4 ± 6.3	422.7 ± 7.4		408 ± 26
6583.39	[N II]	2.25	95.4 ± 4.5	60.3 ± 3.9	51.8 ± 3.9		30.1 ± 6.0
6678.149	He I	2.20	10.1 ± 1.7	5.5 ± 1.1	6.10.9		
6716.42	[S II]	2.18	12.7 ± 1.8	4.6 ± 1.0	< 3		< 12
6730.78	[S II]	2.17	14.1 ± 1.8	6.7 ± 1.1	< 3		< 12
7065.188	He I	2.01	9.1 ± 2.2	14.0 ± 2.0	16.4 ± 4.0		
7135.8	[Ar III]	1.98	39.7 ± 2.8	23.2 ± 2.1	14.9 ± 4.0		
7319.92	[O II]	1.90	12.6 ± 2.2	10.8 ± 1.9			
7330.19	[O II]	1.90	6.5 ± 2.1	6.9 ± 1.8			
$E(B - V)_{H\alpha}$	(mag)		0.42 ± 0.03	0.35 ± 0.02	0.37 ± 0.02		0.36 ± 0.06
$E(B - V)_{H\gamma}$	(mag)		0.44 ± 0.20	0.43 ± 0.12	0.52 ± 0.19	0.00 ± 0.17	0.76 ± 0.50

^aThe scale is such that $F(H\beta) = 100$. If no uncertainty is quoted, the value is a 2σ upper limit to the line intensity.

^b $A_1(\lambda)$ is the extinction for a reddening $E(B - V) = 1$ mag, derived from the Fitzpatrick (1999) reddening law parametrized with a ratio of total-to-selective extinction of 3.041.

TABLE 5
OBSERVED LINE INTENSITIES^a FOR PNE IN M32

Wavelength	Ion	$A_1(\lambda)^b$	PN3	PN5	PN1	PN4, M31	PN17, M31	M3273, M31
3727	[O II]	4.52	22.8 ± 7.9	22.6 ± 5.3	38.9 ± 8.1	44 ± 13		< 91
3868.76	[Ne III]	4.39	103.8 ± 7.7	87.1 ± 5.4	68.4 ± 5.9	77.9 ± 9.7	43.3 ± 6.5	72 ± 22
3889.049	H I	4.37		14.4 ± 4.1	15.3 ± 4.6	15.8 ± 7.3	18.5 ± 5.3	
3967.47	[Ne III]	4.30	29.2 ± 7.1	27.5 ± 5.5	10.7 ± 6.1	19 ± 10	14.3 ± 6.7	
3970.072	H I	4.29	12.6 ± 6.7	15.3 ± 5.2	21.7 ± 6.4	26 ± 11	12.3 ± 6.6	
4101.765	H I	4.18	26.4 ± 5.2	17.1 ± 3.0	26.2 ± 4.0	20.2 ± 4.6	10.8 ± 3.6	
4340.495	H I	3.97	45.1 ± 4.5	40.7 ± 2.9	42.1 ± 3.5	46.4 ± 3.5	34.2 ± 4.2	37.2 ± 8.8
4363.21	[O III]	3.95	14.9 ± 3.6	6.0 ± 2.1	< 5	16.5 ± 2.9	< 7	15.6 ± 7.0
4471.477	He I	3.86	7.1 ± 3.2	4.4 ± 2.1	4.2 ± 2.4	4.1 ± 2.4	4.7 ± 3.0	
4685.75	He II	3.66	< 7	7.6 ± 2.0	4.9 ± 1.8	46.7 ± 3.6	< 4	87 ± 12
4711.34	[Ar IV]	3.63				7.1 ± 2.7		
4740.2	[Ar IV]	3.60				6.9 ± 2.7		
4861.332	H I	3.49	100.0 ± 4.0	100.0 ± 2.8	100.0 ± 2.5	100.0 ± 2.5	100.0 ± 3.4	100.0 ± 9.5
4958.92	[O III]	3.39	418 ± 13	432.8 ± 9.5	317.4 ± 6.1	571 ± 11	281.2 ± 8.6	433 ± 30
5006.85	[O III]	3.34	1262 ± 36	1325 ± 26	967 ± 16	1738 ± 29	863 ± 20	1278 ± 80
5200	[N I]	3.19			5.2 ± 1.4			
5754.57	[N II]	2.75	9.6 ± 2.5		7.7 ± 1.7			
5875.666	He I	2.65	22.5 ± 3.1	21.1 ± 2.8	17.8 ± 2.0	19.0 ± 3.4	19.1 ± 2.1	< 15
6548.06	[N II]	2.26	102 ± 10	40.0 ± 5.3	90.4 ± 6.1	20.3 ± 4.3		27.5 ± 9.0
6562.817	H I	2.26	324 ± 14	345.1 ± 9.2	316.9 ± 8.6	295.3 ± 7.2	423 ± 16	282 ± 21
6583.39	[N II]	2.25	309 ± 14	122.7 ± 6.1	261.5 ± 7.9	49.6 ± 4.5	108 ± 11	40.3 ± 9.3
6678.149	He I	2.20		4.5 ± 1.4	4.0 ± 1.2			
6716.42	[S II]	2.18	< 4	3.6 ± 1.3	12.8 ± 1.4	< 4	< 5	< 14
6730.78	[S II]	2.17	< 4	11.2 ± 1.7	19.6 ± 1.5	< 4	< 5	< 14
7065.188	He I	2.01	10.9 ± 2.5	6.4 ± 1.9	4.9 ± 1.2	5.3 ± 1.7	19.3 ± 3.0	
7135.8	[Ar III]	1.98	27.2 ± 3.1	29.4 ± 2.5	17.1 ± 1.6	15.3 ± 2.1	40.2 ± 3.5	31.8 ± 8.8
7319.92	[O II]	1.90					27.6 ± 3.6	
7330.19	[O II]	1.90					21.2 ± 3.5	
$E(B - V)_{H\alpha}$	(mag)		0.13 ± 0.07	0.16 ± 0.05	0.09 ± 0.05	0.04 ± 0.04	0.36 ± 0.06	0.01 ± 0.15
$E(B - V)_{H\gamma}$	(mag)		0.10 ± 0.31	0.31 ± 0.22	0.24 ± 0.24	0.03 ± 0.22	0.71 ± 0.35	0.53 ± 0.75

^aThe scale is such that $F(H\beta) = 100$. If no uncertainty is quoted, the value is a 2σ upper limit to the line intensity.

^b $A_1(\lambda)$ is the extinction for a reddening $E(B - V) = 1$ mag, derived from the Fitzpatrick (1999) reddening law parametrized with a ratio of total-to-selective extinction of 3.041.

TABLE 6
OBSERVED LINE INTENSITIES^a FOR PNE IN M32 (CONT)

Wavelength	Ion	$A_1(\lambda)^b$	PN30	PN8	PN11	PN29	PN2	PN22	PN7	PN21
3727	[O II]	4.52	53 ± 15		152 ± 25	< 84		< 85	46 ± 11	33 ± 14
3868.76	[Ne III]	4.39	81 ± 11		< 26	93 ± 13		92 ± 18	41.7 ± 4.7	123 ± 20
3889.049	H I	4.37			24 ± 13	26 ± 10			10.9 ± 3.7	
3967.47	[Ne III]	4.30	38.3 ± 9.6	8.2 ± 2.5	22 ± 13	17 ± 13		35 ± 18	21.6 ± 5.0	60 ± 15
3970.072	H I	4.29				15 ± 13		17 ± 17	6.2 ± 4.5	
4101.765	H I	4.18	25.7 ± 6.2	13.7 ± 3.0	23.0 ± 4.5	29.3 ± 5.5	28.4 ± 5.8	25.6 ± 8.1	21.0 ± 2.4	
4340.495	H I	3.97	46.0 ± 4.6	43.9 ± 1.7	43.8 ± 4.5	32.7 ± 4.4	40.3 ± 3.1	49.0 ± 7.6	44.3 ± 1.8	62 ± 13
4363.21	[O III]	3.95	6.8 ± 3.2	10.9 ± 1.4	< 7.1	12.6 ± 3.7	10.1 ± 2.4	15.0 ± 6.3	3.8 ± 1.3	20 ± 10
4471.477	He I	3.86	10.6 ± 3.5	3.7 ± 1.2	6.6 ± 3.2				6.4 ± 1.4	
4685.75	He II	3.66	< 6	4.3 ± 1.2	5.4 ± 3.1	13.4 ± 3.7	31.5 ± 3.2	< 19	< 3	26.1 ± 8.2
4711.34	[Ar IV]	3.63		3.6 ± 1.1			6.8 ± 2.5			
4740.2	[Ar IV]	3.60		3.6 ± 1.1			7.6 ± 2.6			
4861.332	H I	3.49	100.0 ± 4.3	100.0 ± 1.7	100.0 ± 3.8	100.0 ± 4.2	100.0 ± 3.2	100.0 ± 6.5	100.0 ± 1.7	100 ± 10
4958.92	[O III]	3.39	298 ± 10	392.7 ± 6.7	102.2 ± 4.3	399 ± 13	487 ± 14	469 ± 23	274.7 ± 4.9	535 ± 44
5006.85	[O III]	3.34	900 ± 27	1172 ± 15	305.0 ± 8.9	1218 ± 36	1462 ± 35	1307 ± 61	821 ± 10	1636 ± 129
5754.57	[N II]	2.75		3.1 ± 1.0						
5875.666	He I	2.65	19.3 ± 3.3	16.0 ± 1.4	17.4 ± 2.6	13.1 ± 3.8	10.9 ± 2.5	13.7 ± 5.1	21.8 ± 1.8	23.2 ± 9.0
6300.32	[O I]	2.40		18.1 ± 1.9			10.7 ± 2.0			
6363.81	[O I]	2.36		2.7 ± 1.3			4.8 ± 1.6			
6548.06	[N II]	2.26		63.5 ± 5.8	75.4 ± 7.0		39.6 ± 6.0		4.4 ± 1.0	106 ± 19
6562.817	H I	2.26	299.4 ± 9.5	313.3 ± 7.8	335 ± 12	288 ± 11	320 ± 10	312 ± 17	329.7 ± 4.1	374 ± 36
6583.39	[N II]	2.25	10.1 ± 2.8	179.8 ± 6.7	205.6 ± 9.1	4.2 ± 5.1	110.5 ± 6.7	4.0 ± 6.5	13.1 ± 1.1	370 ± 35
6678.149	He I	2.20		3.6 ± 1.3	8.0 ± 2.1	< 6	5.0 ± 1.7		6 ± 1.2	
6716.42	[S II]	2.18	< 4	15.4 ± 1.7	19.5 ± 2.4	< 6	11.0 ± 1.9	< 10	< 2	< 26
6730.78	[S II]	2.17	< 4	18.9 ± 1.7	24.5 ± 2.6	< 6	16.8 ± 2.0			
7065.188	He I	2.01		7.0 ± 1.5		3.1 ± 2.1	6.6 ± 2.9			
7135.8	[Ar III]	1.98		26.4 ± 1.9	12.5 ± 2.1	11.5 ± 2.6	31.7 ± 3.8			36.3 ± 9.7
7319.92	[O II]	1.90		< 5	14.0 ± 3.2		9.7 ± 3.0			
7330.19	[O II]	1.90		< 5	5.4 ± 2.4		5.9 ± 2.8			
$E(B - V)_{H\alpha}$	(mag)			0.09 ± 0.04	0.17 ± 0.06	0.02 ± 0.07	0.10 ± 0.06	0.09 ± 0.11		0.25 ± 0.18
$E(B - V)_{H\gamma}$	(mag)		0.05 ± 0.32	0.15 ± 0.13	0.18 ± 0.31	0.81 ± 0.40	0.34 ± 0.24	0.00 ± 0.50	0.12 ± 0.13	0.00 ± 0.72

^aThe scale is such that $F(H\beta) = 100$. If no uncertainty is quoted, the value is a 2σ upper limit to the line intensity.

^b $A_1(\lambda)$ is the extinction for a reddening $E(B - V) = 1$ mag, derived from the Fitzpatrick (1999) reddening law parametrized with a ratio of total-to-selective extinction of 3.041.

TABLE 7
CHEMICAL ABUNDANCES FOR PNE IN NGC 185

Quantity	Lines Used	PN3	PN5	PN1	PN2	PN4
T_e	4363/5007	15100 ⁺¹⁵⁰⁰ ₋₁₄₀₀	16400 ⁺²³⁰⁰ ₋₂₁₀₀	17200 ⁺⁵⁰⁰ ₋₅₀₀	9300 ⁺⁹⁰⁰ ₋₁₀₀₀	15100 ⁺²⁶⁰⁰ ₋₂₃₀₀
N_e	6716/6731	2000	2000	2000	2000	2000
He ⁺ /H	5876	0.058 ^{+0.011} _{-0.011}	0.089 ^{+0.020} _{-0.019}	0.104 ^{+0.004} _{-0.004}	0.108 ^{+0.006} _{-0.007}	0.094 ^{+0.026} _{-0.025}
He ²⁺ /H	4686	0.040 ^{+0.005} _{-0.005}	0.012 ^{+0.004} _{-0.003}	0.008 ^{+0.001} _{-0.001}	0.002	0.010
10 ⁶ N ⁺ /H	6584	9.6 ^{+2.1} _{-1.6}	1.22 ^{+0.57} _{-0.38}	1.4 ^{+1.3} _{-1.2}	8.7 ^{+3.8} _{-2.1}	0.50 ^{+0.26} _{-0.15}
10 ⁵ O ⁺ /H	3727	0.39 ^{+0.49} _{-0.28}	0.21 ^{+0.12} _{-0.07}	0.09 ^{+0.04} _{-0.03}	2.7 ^{+3.2} _{-1.3}	0.87 ^{+0.70} _{-0.35}
10 ⁵ O ⁺ /H	7325			0.55 ^{+0.18} _{-0.15}		
10 ⁵ O ²⁺ /H	5007	17.0 ^{+5.5} _{-3.8}	7.4 ^{+3.2} _{-2.0}	8.05 ^{+0.57} _{-0.53}	30 ⁺¹⁸ ₋₉	11.8 ^{+7.3} _{-4.1}
10 ⁵ Ne ²⁺ /H	3869	3.4 ^{+1.9} _{-1.2}	0.90 ^{+0.78} _{-0.42}	1.68 ^{+0.21} _{-0.19}	5.1 ^{+4.7} _{-2.1}	1.8 ^{+2.2} _{-1.0}
ICF(N)		63.51	39.95	87.97	12.48	15.50
ICF(O)		1.42	1.09	1.05	1.01	1.07
ICF(Ne)		1.45	1.12	1.06	1.10	1.15
He/H		0.098 ^{+0.012} _{-0.012}	0.101 ^{+0.020} _{-0.019}	0.112 ^{+0.004} _{-0.004}	0.110 ^{+0.006} _{-0.007}	0.103 ^{+0.026} _{-0.025}
12 + log(N/H)		8.79 ^{+0.10} _{-0.07}	7.69 ^{+0.20} _{-0.14}	8.08 ^{+0.04} _{-0.04}	8.03 ^{+0.19} _{-0.10}	6.89 ^{+0.23} _{-0.13}
12 + log(O/H)		8.39 ^{+0.14} _{-0.09}	7.92 ^{+0.18} _{-0.11}	7.93 ^{+0.03} _{-0.03}	8.52 ^{+0.24} _{-0.12}	8.13 ^{+0.25} _{-0.14}
12 + log(Ne/H)		7.69 ^{+0.25} _{-0.16}	7.00 ^{+0.38} _{-0.20}	7.25 ^{+0.05} _{-0.05}	7.75 ^{+0.40} _{-0.17}	7.31 ^{+0.54} _{-0.24}
log(N/O)		0.39 ^{+0.56} _{-0.32}	-0.23 ^{+0.32} _{-0.19}	0.15 ^{+0.16} _{-0.14}	-0.48 ^{+0.56} _{-0.24}	-1.24 ^{+0.41} _{-0.22}
log(Ne/O)		-0.70 ^{+0.28} _{-0.18}	-0.91 ^{+0.42} _{-0.23}	-0.68 ^{+0.06} _{-0.06}	-0.77 ^{+0.47} _{-0.21}	-0.82 ^{+0.60} _{-0.29}

TABLE 8
CHEMICAL ABUNDANCES FOR PNE IN NGC 205

Quantity	Lines Used	PN2	PN3	PN26	PN10	PN1	PN9	PN8
T_e	4363/5007	< 15900	13300 ⁺⁴¹⁰⁰ ₋₃₅₀₀	< 16600	< 15600	11500 ⁺²⁶⁰⁰ ₋₂₄₀₀	< 15200	17700 ⁺³⁵⁰⁰ ₋₂₉₀₀
N_e	6716/6731	2000	2000	2000	2000	2000	2000	2000
He ⁺ /H	5876	0.140 ^{+0.022} _{-0.023}	0.149 ^{+0.021} _{-0.022}	0.093 ^{+0.015} _{-0.015}	0.093 ^{+0.023} _{-0.024}	0.128 ^{+0.007} _{-0.014}	0.091 ^{+0.017} _{-0.018}	0.095 ^{+0.017} _{-0.018}
He ²⁺ /H	4686	< 0.005	< 0.003	< 0.008	< 0.016	0.003 ^{+0.002} _{-0.002}	< 0.012	0.007 ^{+0.005} _{-0.004}
10 ⁶ N ⁺ /H	6584	0.36 ^{+0.31} _{-0.30}	2.2 ^{+3.0} _{-1.1}	1.75 ^{+0.21} _{-0.21}	2.36 ^{+0.33} _{-0.34}	4.1 ^{+4.6} _{-1.9}	2.30 ^{+0.31} _{-0.31}	0.53 ^{+0.34} _{-0.22}
10 ⁵ O ⁺ /H	3727	1.50 ^{+0.96} _{-0.72}	0.64 ^{+3.2} _{-0.52}	< 0.45		2.23 ^{+7.6} _{-1.6}	< 1.9	< 0.47
10 ⁵ O ²⁺ /H	7325			0.97 ^{+0.47} _{-0.41}			1.11 ^{+0.27} _{-0.22}	
10 ⁵ O ²⁺ /H	5007	11.6 ^{+1.9} _{-1.8}	6.3 ^{+10.0} _{-3.1}	4.98 ^{+0.73} _{-0.67}	10.6 ^{+1.7} _{-1.6}	14 ⁺¹⁶ ₋₆	10.0 ^{+1.4} _{-1.3}	8.0 ^{+4.8} _{-2.8}
10 ⁵ Ne ²⁺ /H	3869	1.65 ^{+0.30} _{-0.28}		1.01 ^{+0.16} _{-0.14}		2.5 ^{+7.4} _{-1.8}	3.0 ^{+1.5} _{-1.2}	
ICF(N)		8.95	10.87	12.79		7.24	6.90	19.07
ICF(O)		< 1.02	< 1.01	< 1.05	< 1.11	1.02	< 1.09	1.05
ICF(Ne)		1.16	1.12	1.15	1.11	1.18	1.29	
He/H		0.145 ^{+0.022} _{-0.023}	0.152 ^{+0.021} _{-0.022}	0.101 ^{+0.015} _{-0.015}	0.109 ^{+0.023} _{-0.024}	0.131 ^{+0.007} _{-0.014}	0.103 ^{+0.017} _{-0.018}	0.102 ^{+0.018} _{-0.018}
12 + log(N/H)		6.50 ^{+0.37} _{-0.36}	7.37 ^{+0.62} _{-0.62}	7.35 ^{+0.05} _{-0.05}		7.47 ^{+0.49} _{-0.20}	7.20 ^{+0.06} _{-0.05}	7.00 ^{+0.28} _{-0.18}
12 + log(O/H)		8.13 ^{+0.09} _{-0.06}	7.85 ^{+0.66} _{-0.20}	7.76 ^{+0.05} _{-0.05}	8.07 ^{+0.07} _{-0.06}	8.21 ^{+0.49} _{-0.17}	8.11 ^{+0.05} _{-0.05}	7.95 ^{+0.25} _{-0.14}
12 + log(Ne/H)		7.28 ^{+0.08} _{-0.07}		7.06 ^{+0.07} _{-0.06}		7.48 ^{+1.27} _{-0.30}	7.58 ^{+0.22} _{-0.18}	
log(N/O)		-1.62 ^{+0.47} _{-0.42}	-0.48 ^{+2.27} _{-0.41}	-0.41 ^{+0.05} _{-0.05}		-0.74 ^{+1.55} _{-0.38}	-0.91 ^{+0.06} _{-0.06}	-0.95 ^{+0.28} _{-0.18}
log(Ne/O)		-0.85 ^{+0.11} _{-0.10}		-0.69 ^{+0.09} _{-0.08}		-0.73 ^{+1.37} _{-0.36}	-0.53 ^{+0.23} _{-0.19}	

Quantity	Lines Used	PN7	PN6	PN5	PN4	PN24	PN19
T_e	4363/5007	11900 ⁺¹¹⁰⁰ ₋₁₁₀₀	14400 ⁺¹³⁰⁰ ₋₁₂₀₀	11100 ⁺⁶⁰⁰ ₋₇₀₀	15100 ⁺¹²⁰⁰ ₋₁₁₀₀	< 16200	< 25000 ^a
N_e	6716/6731	2000	2000	2000	2000	2000	2000
He ⁺ /H	5876	0.118 ^{+0.010} _{-0.010}	0.065 ^{+0.009} _{-0.009}	0.092 ^{+0.006} _{-0.006}	0.111 ^{+0.010} _{-0.010}	0.063 ^{+0.002} _{-0.005}	0.047 ^{+0.002} _{-0.002}
He ²⁺ /H	4686	< 0.003	0.023 ^{+0.003} _{-0.003}	0.005 ^{+0.001} _{-0.001}	0.011 ^{+0.002} _{-0.002}	< 0.003	0.027 ^{+0.008} _{-0.008}
10 ⁶ N ⁺ /H	6584	2.51 ^{+0.93} _{-0.62}	5.0 ^{+1.0} _{-0.8}	6.1 ^{+1.4} _{-1.0}	2.63 ^{+0.60} _{-0.47}		0.66 ^{+0.09} _{-0.10}
10 ⁵ O ⁺ /H	3727	< 6.8		0.94 ^{+0.62} _{-0.39}	2.4 ^{+0.21} _{-0.13}	1.17 ^{+0.66} _{-0.44}	< 0.5
10 ⁵ O ⁺ /H	7325	2.5 ^{+2.9} _{-1.3}	1.5 ^{+1.1} _{-0.6}	5.4 ^{+3.7} _{-2.2}			
10 ⁵ O ²⁺ /H	5007	19.0 ^{+7.5} _{-4.6}	15.8 ^{+4.4} _{-3.3}	31.9 ^{+7.5} _{-5.3}	12.3 ^{+2.9} _{-2.1}	2.30 ^{+0.34} _{-0.34}	1.47 ^{+0.08} _{-0.08}
10 ⁵ Ne ²⁺ /H	3869	2.2 ^{+1.7} _{-0.9}	9.2 ^{+6.9} _{-4.4}	4.8 ^{+1.9} _{-1.3}	1.29 ^{+0.69} _{-0.46}		
ICF(N)		29.34		36.26	56.51	3.05	5.40
ICF(O)		< 1.01	1.22	1.04	1.06	< 1.03	1.36
ICF(Ne)		1.05	1.22	1.07	1.08	1.56	1.81
He/H		0.121 ^{+0.010} _{-0.010}	0.089 ^{+0.010} _{-0.010}	0.097 ^{+0.006} _{-0.006}	0.122 ^{+0.010} _{-0.010}	0.066 ^{+0.002} _{-0.005}	0.074 ^{+0.008} _{-0.008}
12 + log(N/H)		7.87 ^{+0.16} _{-0.11}		8.34 ^{+0.10} _{-0.07}	8.17 ^{+0.10} _{-0.08}		6.55 ^{+0.06} _{-0.06}
12 + log(O/H)		8.30 ^{+0.17} _{-0.10}	8.33 ^{+0.11} _{-0.08}	8.53 ^{+0.10} _{-0.07}	8.12 ^{+0.10} _{-0.07}	7.55 ^{+0.09} _{-0.07}	7.42 ^{+0.02} _{-0.02}
12 + log(Ne/H)		7.37 ^{+0.33} _{-0.18}	7.05 ^{+0.33} _{-0.21}	7.71 ^{+0.17} _{-0.11}	7.15 ^{+0.23} _{-0.16}		
log(N/O)		-0.43 ^{+0.16} _{-0.11}		-0.19 ^{+0.30} _{-0.20}	0.05 ^{+0.39} _{-0.26}		-0.87 ^{+0.06} _{-0.06}
log(Ne/O)		-0.93 ^{+0.37} _{-0.21}	-1.24 ^{+0.35} _{-0.23}	-0.82 ^{+0.20} _{-0.13}	-0.98 ^{+0.25} _{-0.17}		

^aThis limit is arbitrary since the line ratio implies an unphysical temperature.

TABLE 9
CHEMICAL ABUNDANCES FOR PNE IN M32

Quantity	Lines Used	PN30	PN8	PN11	PN29	PN2	PN22	PN7	PN21
T_e	4363/5007	12300 ⁺²⁶⁰⁰ ₋₂₅₀₀	11400 ⁺⁶⁰⁰ ₋₆₀₀	< 16900	11600 ⁺¹⁴⁰⁰ ₋₁₅₀₀	10400 ⁺⁹⁰⁰ ₋₉₀₀	12300 ⁺²³⁰⁰ ₋₂₃₀₀	9200 ⁺¹⁰⁰⁰ ₋₁₁₀₀	12900 ⁺³⁴⁰⁰ ₋₃₂₀₀
N_e	6716/6731	2000	2000	2000	2000	2000	2000	2000	2000
He ⁺ /H	5876	< 0.100	0.100 ^{+0.011} _{-0.010}	0.090 ^{+0.015} _{-0.015}	0.086 ^{+0.031} _{-0.028}	0.069 ^{+0.017} _{-0.018}	0.084 ^{+0.042} _{-0.035}	0.136 ^{+0.004} _{-0.007}	0.123 ^{+0.070} _{-0.055}
He ²⁺ /H	4686	0.073 ^{+0.022} _{-0.019}	0.004 ^{+0.001} _{-0.001}	0.005 ^{+0.003} _{-0.003}	0.011 ^{+0.004} _{-0.004}	0.026 ^{+0.004} _{-0.004}	< 0.016	< 0.002	0.023 ^{+0.012} _{-0.010}
10 ⁶ N ⁺ /H	6584	4.8 ^{+5.9} _{-2.4}	23.2 ^{+4.0} _{-3.3}	10.6 ^{+0.9} _{-0.9}	0.56 ^{+1.3} _{-0.65}	17.6 ^{+6.2} _{-4.1}	0.43 ^{+1.5} _{-0.62}	2.8 ^{+1.2} _{-0.7}	29 ⁺³⁵ ₋₁₃
10 ⁵ O ⁺ /H	3727	< 2.0		1.41 ^{+0.46} _{-0.38}	< 2.3		< 2.0	3.7 ^{+5.7} _{-2.1}	0.76 ^{+3.2} _{-0.59}
10 ⁵ O ²⁺ /H	7325		3.7 ^{+1.3} _{-0.9}	1.13 ^{+0.44} _{-0.40}		10 ⁺¹⁴ ₋₆			
10 ⁵ O ²⁺ /H	5007	23 ⁺³³ ₋₁₁	26.4 ^{+5.6} _{-4.5}	2.34 ^{+0.28} _{-0.26}	26 ⁺¹⁶ ₋₈	44 ⁺²⁰ ₋₁₂	23 ⁺²⁷ ₋₁₀	37 ⁺²⁴ ₋₁₂	25 ⁺⁴⁶ ₋₁₃
10 ⁵ Ne ²⁺ /H	3869	3.6 ^{+9.4} _{-2.4}		0.58	5.7 ^{+5.9} _{-2.6}		5.0 ^{+9.7} _{-2.9}	7.1 ^{+3.4} _{-3.4}	6.5 ⁺¹⁹ _{-4.2}
ICF(N)		18.00	8.32	2.75	13.21	6.62	13.99	11.20	37.50
ICF(O)		< 1.44	1.02	1.04	1.08	1.24	< 1.12	< 1.01	1.12
ICF(Ne)		1.57	1.02	1.66	1.18	1.52	1.22	1.11	1.16
He/H		0.173 ^{+0.022} _{-0.019}	0.103 ^{+0.011} _{-0.010}	0.095 ^{+0.016} _{-0.015}	0.097 ^{+0.032} _{-0.028}	0.095 ^{+0.018} _{-0.018}	0.100 ^{+0.042} _{-0.035}	0.138 ^{+0.004} _{-0.007}	0.146 ^{+0.071} _{-0.056}
12 + log(N/H)		7.93 ^{+0.54} _{-0.27}	8.29 ^{+0.07} _{-0.06}	7.46 ^{+0.04} _{-0.04}	6.87 ^{+0.90} _{-0.59}	8.07 ^{+0.15} _{-0.10}	6.78 ^{+1.51} _{-0.63}	7.50 ^{+0.19} _{-0.11}	9.04 ^{+0.52} _{-0.19}
12 + log(O/H)		8.55 ^{+0.57} _{-0.19}	8.49 ^{+0.08} _{-0.07}	7.59 ^{+0.06} _{-0.05}	8.48 ^{+0.25} _{-0.13}	8.83 ^{+0.19} _{-0.11}	8.45 ^{+0.47} _{-0.17}	8.62 ^{+0.26} _{-0.13}	8.45 ^{+0.79} _{-0.23}
12 + log(Ne/H)		7.75 ^{+1.14} _{-0.29}		6.98	7.83 ^{+0.45} _{-0.20}		7.79 ^{+0.84} _{-0.25}	7.90 ^{+0.50} _{-0.21}	7.87 ^{+1.25} _{-0.28}
log(N/O)		-0.62 ^{+0.54} _{-0.22}	-0.20 ^{+0.17} _{-0.13}	-0.13 ^{+0.15} _{-0.12}	-1.61 ^{+0.90} _{-0.50}	-0.76 ^{+0.62} _{-0.28}	-1.67 ^{+1.51} _{-0.63}	-1.12 ^{+0.69} _{-0.27}	0.59 ^{+1.91} _{-0.39}
log(Ne/O)		-0.80 ^{+1.30} _{-0.36}		-0.61 ^{+0.05} _{-0.05}	-0.65 ^{+0.52} _{-0.24}		-0.67 ^{+0.98} _{-0.32}	-0.72 ^{+0.57} _{-0.25}	-0.58 ^{+1.49} _{-0.37}

Quantity	Lines Used	PN3	PN5	PN1	PN4, M31	PN17, M31	M3273, M31
T_e	4363/5007	12500 ⁺¹⁴⁰⁰ ₋₁₄₀₀	9200 ⁺¹⁰⁰⁰ ₋₁₁₀₀	< 9400	11400 ⁺⁸⁰⁰ ₋₈₀₀	< 11245	10500 ⁺²²⁰⁰ ₋₂₁₀₀
N_e	6716/6731	2000	2000	2000	2000	2000	2000
He ⁺ /H	5876	0.132 ^{+0.026} _{-0.023}	0.128 ^{+0.019} _{-0.020}	0.114 ^{+0.014} _{-0.013}	0.123 ^{+0.027} _{-0.025}	0.098 ^{+0.012} _{-0.012}	0.127 ^{+0.002} _{-0.008}
He ²⁺ /H	4686	< 0.006	0.006 ^{+0.002} _{-0.002}	0.004 ^{+0.002} _{-0.002}	0.039 ^{+0.005} _{-0.004}	< 0.004	< 0.005
10 ⁶ N ⁺ /H	6584	3.1 ^{+1.1} _{-0.7}	25 ⁺¹³ ₋₇	54.5 ^{+3.2} _{-2.5}	6.8 ^{+2.1} _{-1.5}	10.5 ^{+1.5} _{-1.5}	1.6 ^{+1.5} _{-0.7}
10 ⁵ O ⁺ /H	3727	0.53 ^{+0.66} _{-0.31}	1.9 ^{+2.6} _{-1.0}	2.7 ^{+0.9} _{-0.7}	1.4 ^{+1.1} _{-0.7}		2.2 ^{+8.3} _{-1.6}
10 ⁵ O ⁺ /H	7325					14.1 ^{+3.1} _{-3.0}	
10 ⁵ O ²⁺ /H	5007	21 ⁺¹¹ ₋₆	59 ⁺⁴⁰ ₋₂₀	40.4 ^{+3.2} _{-2.5}	39 ⁺¹² ₋₈	19.4 ^{+2.0} _{-2.0}	26 ⁺³⁵ ₋₁₂
10 ⁵ Ne ²⁺ /H	3869	5.5 ^{+4.1} _{-2.1}	15 ⁺¹⁵ ₋₆	10.2 ^{+1.9} _{-1.6}	5.3 ^{+2.9} _{-1.8}	4.0 ^{+1.2} _{-1.0}	7.5 ⁺²¹ _{-4.9}
ICF(N)		42.24	33.52	16.13	36.02	2.43	13.11
ICF(O)		< 1.03	1.03	1.02	1.20	< 1.03	< 1.03
ICF(Ne)		1.05	1.06	1.09	1.24	1.77	1.11
He/H		0.138 ^{+0.026} _{-0.023}	0.134 ^{+0.019} _{-0.020}	0.118 ^{+0.014} _{-0.014}	0.162 ^{+0.027} _{-0.025}	0.101 ^{+0.012} _{-0.012}	0.133 ^{+0.002} _{-0.008}
12 + log(N/H)		9.11 ^{+0.16} _{-0.10}	8.92 ^{+0.22} _{-0.12}	8.94 ^{+0.03} _{-0.02}	8.39 ^{+0.13} _{-0.10}	7.41 ^{+0.06} _{-0.06}	7.34 ^{+0.39} _{-0.19}
12 + log(O/H)		8.35 ^{+0.22} _{-0.13}	8.80 ^{+0.28} _{-0.14}	8.64 ^{+0.03} _{-0.03}	8.69 ^{+0.13} _{-0.09}	8.54 ^{+0.05} _{-0.05}	8.46 ^{+0.55} _{-0.19}
12 + log(Ne/H)		7.76 ^{+0.32} _{-0.17}	8.21 ^{+0.42} _{-0.18}	8.05 ^{+0.08} _{-0.07}	7.82 ^{+0.24} _{-0.15}	7.85 ^{+0.13} _{-0.11}	7.92 ^{+1.22} _{-0.28}
log(N/O)		0.76 ^{+0.56} _{-0.27}	0.12 ^{+0.64} _{-0.26}	0.30 ^{+0.15} _{-0.12}	-0.30 ^{+0.39} _{-0.23}	-1.13 ^{+0.11} _{-0.11}	-1.13 ^{+1.67} _{-0.37}
log(Ne/O)		-0.59 ^{+0.39} _{-0.21}	-0.59 ^{+0.51} _{-0.23}	-0.60 ^{+0.09} _{-0.07}	-0.87 ^{+0.27} _{-0.17}	-0.68 ^{+0.13} _{-0.12}	-0.54 ^{+1.35} _{-0.35}

TABLE 11
IONIC ABUNDANCES FOR PNE FROM THE LITERATURE

Galaxy	PN ID	T_e	He^0/H	He^+/H	$10^5 \times \text{O}^+/\text{H}$	$10^5 \times \text{O}^{++}/\text{H}$	$10^6 \times \text{N}^+/\text{H}$	$10^5 \times \text{Ne}^{++}/\text{H}$	Ref ^a
Leo A	PN01	20819 ⁺¹⁹⁰³ ₋₁₆₇₇	0.108 ^{+0.026} _{-0.025}	0.019 ^{+0.002} _{-0.002}	0.0373 ^{+0.0101} _{-0.0077}	1.9 ^{+0.52} _{-0.4}	0.101 ^{+0.035} _{-0.027}	0.311 ^{+0.108} _{-0.08}	1
Sextans A	PN01	20546 ⁺¹⁴⁴⁸ ₋₁₄₁₅	0.044 ^{+0.009} _{-0.009}	0.045 ^{+0.003} _{-0.003}	1.05 ^{+0.82} _{-0.5}	3.24 ^{+0.64} _{-0.48}	35.8 ⁺⁶ _{-4.2}	0.213 ^{+0.119} _{-0.089}	2,3
Sextans B	PN01	13025 ⁺²⁷⁶⁵ ₋₂₉₀₁	0.087 ^{+0.026} _{-0.019}	0.0009 ^{+0.0001} _{-0.0001}	0.342 ^{+0.649} _{-0.173}	8.91 ^{+11.2} _{-3.7}	0.195 ^{+0.169} _{-0.065}	1.66 ^{+4.04} _{-1.03}	2
Sextans B	PN02	16295 ⁺²⁸⁴⁶ ₋₂₇₁₁	0.083 ^{+0.037} _{-0.03}	0.0026 ^{+0.0002} _{-0.0002}	0.59 ^{+1.146} _{-0.394}	4.85 ^{+3.15} _{-1.59}	0.447 ^{+0.207} _{-0.117}	0.619 ^{+0.811} _{-0.336}	2
Sextans B	PN03	20746 ⁺³⁷⁰⁹ ₋₃₃₃₀	0.059 ^{+0.011} _{-0.009}	0.0018 ⁺⁰ ₋₀	0.657 ^{+0.747} _{-0.237}	2.05 ^{+1.42} _{-0.72}	0.241 ^{+0.215} _{-0.121}	0.712 ^{+0.513} _{-0.271}	2,3
Sextans B	PN04	11206 ⁺²⁷⁶⁴ ₋₃₄₁₉	0.086 ^{+0.023} _{-0.025}	0.0008 ^{+0.0001} _{-0.0001}	4.66 ^{+51.4} _{-3.29}	18.7 ^{+54.7} _{-9.2}	0.522 ^{+1.948} _{-0.439}	3.3 ^{+17.49} _{-2.12}	2
Sextans B	PN05	12534 ⁺⁹⁰⁹ ₋₈₈₈	0.115 ^{+0.016} _{-0.015}	0.0052 ^{+0.0019} _{-0.0019}	0.494 ^{+0.506} _{-0.299}	15.7 ^{+4.2} ₋₃	1.16 ^{+0.34} _{-0.25}	4.95 ^{+2.06} _{-1.37}	2
NGC 6822	S33	19479 ⁺⁸³⁵ ₋₁₂₅₃	0.053 ^{+0.018} _{-0.014}	0.055 ^{+0.002} _{-0.002}	0.254 ^{+0.663} _{-0.125}	6.37 ^{+1.17} _{-0.57}	20.1 ⁺⁶ _{-1.8}	0.648 ^{+0.183} _{-0.113}	2
NGC 6822	pn010	19754 ⁺⁵²²⁰ ₋₄₁₈₃	0.087 ^{+0.026} _{-0.029}	0.034 ^{+0.007} _{-0.007}	1.92 ^{+2.59} _{-1.02}	4.18 ^{+3.25} _{-1.62}	0.967 ^{+0.711} _{-0.395}	0.992 ^{+1.427} _{-0.573}	2
NGC 6822	pn012	14930 ⁺⁵⁴⁵⁶ ₋₄₈₇₇	0.075 ^{+0.029} _{-0.029}	0.012 ^{+0.001} _{-0.001}	1.55 ^{+8.95} _{-1.22}	7.75 ^{+18.41} _{-4.12}	0.493 ^{+1.309} _{-0.377}	2.25 ^{+10.51} _{-1.65}	2
NGC 6822	S16	14019 ⁺¹⁵⁵² ₋₁₄₄₁	0.083 ^{+0.01} _{-0.009}	0.02 ^{+0.003} _{-0.002}	1.34 ^{+1.31} _{-0.66}	14.7 ^{+5.5} _{-3.7}	1.28 ^{+0.69} _{-0.48}	3.02 ^{+1.97} _{-1.16}	2
NGC 6822	pn017	21711 ⁺⁸⁷⁷⁵ ₋₅₈₆₆	0.024 ^{+0.005} _{-0.006}	0.039 ^{+0.013} _{-0.01}	0.987 ^{+2.291} _{-0.603}	3.3 ^{+3.64} _{-1.57}	1.61 ^{+1.37} _{-0.7}	0.679 ^{+0.894} _{-0.349}	2
NGC 6822	pn020	< 15790	0.08 ^{+0.01} _{-0.011}	0.0087 ^{+0.0001} _{-0.0001}	0.617 ^{+0.307} _{-0.27}	7.95 ^{+1.09} _{-1.01}	0.217 ^{+0.028} _{-0.025}	2.63 ^{+1.13} _{-0.95}	2
NGC 6822	pn019	15735 ⁺¹⁴⁹⁹ ₋₁₄₁₉	0.174 ^{+0.011} _{-0.011}	0.002 ⁺⁰ ₋₀	0.0634 ^{+0.0231} _{-0.0156}	4.34 ^{+1.27} _{-0.89}	0.23 ^{+0.221} _{-0.164}	0.637 ^{+0.405} _{-0.257}	2
SMC	MG13	22563		0.107		1.35		0.205	
SMC	SMP17	12060	0.092	0.0013	0.599	15.5	1.11	4.08	
SMC	SMP13	13489	0.08		0.33	11.5	0.467	1.6	
SMC	SMP15	12446	0.126	0.0003	0.251	9.99	1.5	1.87	
SMC	SMP27	12145	0.091		0.438	10.4	0.612	1.46	
SMC	SMP2	13584	0.071	0.024	0.335	11.5	0.767	1.8	
SMC	SMP5	13584	0.069	0.035	1.24	13.1	2.39	3.16	
SMC	SMP20	13348	0.093	0.0003	0.143	5.8	0.378	0.733	
SMC	SMP6	13970	0.104	0.0004	0.151	9.91	3.31	1.89	
SMC	SMP24	10973	0.095		1.77	10.5	2.75	1.49	
SMC	SMP8	12622	0.083		0.213	10.4		1.18	
SMC	SMP14	12889	0.06	0.032	0.751	14.2	1.32	3.49	
SMC	SMP19	13824	0.053	0.035	0.57	10.7	1.13	2.81	
SMC	SMP4	15354	0.114	0.0004	0.0399	6.83	0.195	1.06	
SMC	SMP18	10596	0.086		3.35	8.75	2.38	2.13	
SMC	SMP10	9276	0.074	0.0004	1.74	36.5	3.49	4.65	
SMC	SMP3	13442	0.12	0.0095	0.244	11	0.441	1.56	
SMC	SMP23	12710	0.092	0.0024	0.206	12.9	0.387	2.52	
SMC	SMP21	23123	0.09	0.036	0.135	2.15	3.93	0.909	
SMC	SMP11	11050	0.085		0.918	5.83	2.56	0.287	
SMC	SMP11	17538	0.08		1	2.34	0.965	0.218	
SMC	SMP22	25954	0.057	0.06	0.202	0.863	6.46	0.365	
SMC	SMP9	13117	0.026	0.049	1.26	13.4	2.17	1.95	
SMC	SMP16	11605	0.055		2.75	3.74	1.77	0.166	
SMC	SMP7	18163	0.026	0.0083	0.325	5.89	0.712	1.4	
SMC	SMP25	32812	0.045	0.056	0.0287	0.741	1.09	0.263	
SMC	SMP28	24713	0.08	0.047	0.114	1.03	5.54	0.537	
SMC	SMP26	15035	0.081	0.015	1.87	5.72	21	1.81	
SMC	SP34	15354	0.063	0.009	2.09	4.29	5.87	0.789	
LMC	J15	11444	0.06	0.0057	13.56	16.1	21.6	5.27	
LMC	J31	12403	0.072	0.029	1.51	20.9	9.12	4.99	

TABLE 10
ATOMIC DATA USED

Ion	Transition Probabilities	Collision Strengths
N^+	Wiese et al. (1996)	Lennon & Burke (1994)
O^+	Wiese et al. (1996)	Pradhan (1976)
O^{2+}	Wiese et al. (1996)	McLaughlin & Bell (1993)
Ne^{2+}	Mendoza & Zeippen (1982)	Butler & Burke (1994)
S^{2+}	Kadish & Sigman (1986)	Butler & Zeippen (1994)

TABLE 11—*Continued*

Galaxy	PN ID	T_e	He ^o /H	He ⁺ /H	$10^5 \times \text{O}^+/\text{H}$	$10^5 \times \text{O}^{++}/\text{H}$	$10^6 \times \text{N}^+/\text{H}$	$10^5 \times \text{Ne}^{++}/\text{H}$	Ref ^a
LMC	J33	12800		0.055		14.8		2.88	5
LMC	J41	15571	0.069	0.0066	0.358	5.75		0.484	5
LMC	J5	17910	0.015	0.036	1.17	2.43	14.9	1.71	5
LMC	MA04	16935		0.071	0.231	4.56		0.899	5
LMC	MA06	16699		0.053	2.28	6.06	33.1	1.7	5
LMC	MA10	18744		0.056	2.06	3.65	18.5	2.28	5
LMC	MA12	13348		0.016	4.62	10.9	15.6	3.03	5
LMC	MA13	20673		0.067	1.13	2.75	22.1	1.3	5
LMC	MA15	16013	0.066		2.94	1.91	5.03		5
LMC	MA16	16583		0.082	0.608	6.52	2.8	1.26	5
LMC	MA17	15571	0.063		4.36	4.59	10.3		5
LMC	MA18	14569	0.054	0.04	1.07	10.7	6.11	2.41	5
LMC	MG03	13209			7.26	8.91	12.3	4.5	5
LMC	MG07	12980		0.011	11.73	14	20.6	4.21	5
LMC	MG21	16641		0.094		2.91		0.447	5
LMC	SMP104a	17599	0.023	0.051	0.0635	1.26	0.394	0.463	5
LMC	SMP62	15571	0.085	0.024	0.589	10.5	3.35	2.22	5
LMC	SMP73	12980	0.078	0.028	1.87	19.6	5.87	4.9	5
LMC	SMP99	12622	0.087	0.021	1.99	20.4	12	3.53	5
LMC	SMP78	13776	0.07	0.025	0.949	17	3.69	3.31	5
LMC	SMP92	13163	0.075	0.033	4.31	20.7	6.25	4.34	5
LMC	SMP63	11484	0.091		1.15	21.7	2.54	3.76	5
LMC	SMP81	14117	0.09			16	1.06	2.44	5
LMC	SMP89	13348	0.071	0.011	1.65	18.5	2.26	4.8	5
LMC	SMP47	14417	0.118	0.039	0.808	12.3	21.1	3.84	5
LMC	SMP38	12844	0.098		2.28	16.9	6.1	4.38	5
LMC	SMP75	11646	0.092			20.2	2.6	4.46	5
LMC	SMP53	16410	0.092		0.761	10.7	4.13	2.28	5
LMC	SMP61	11444	0.113		9.18	15.1	8.62	2.62	5
LMC	SMP1	11564	0.147		0.705	18.3	1.98	2.66	5
LMC	SMP74	12403	0.091	0.023	2.46	19.2	4.29	4.43	5
LMC	SMP6	13442	0.057	0.031	1.97	14.2	2.98	3.69	5
LMC	SMP48	13255	0.132		0.784	9.04	3.19	1.69	5
LMC	SMP58	12578	0.084	0.0015	0.163	11.7	0.647	1.56	5
LMC	SMP50	13632	0.092	0.016	0.388	13.3	0.737	2.5	5
LMC	SMP19	13680	0.057	0.04	3.33	15.7	7.34	4.02	5
LMC	SMP76	11324	0.102		0.67	13.5	1.46	2.35	5
LMC	SMP35	13348	0.063	0.016	1.34	17.7	4.6	3.05	5
LMC	SMP29	19962	0.064	0.061	0.29	4.73	16.9	0.995	5
LMC	SMP21	19685	0.062	0.047	0.707	5.08	24.2	1.2	5
LMC	SMP83	17661	0.056	0.052	0.547	6.38	6.65	1.46	5
LMC	SMP33	13302	0.059	0.039	2.78	17.6	8.32	3.68	5
LMC	SMP32	15625	0.045	0.061	1.02	9.12	2.4	1.81	5
LMC	SMP23	11245	0.085		0.65	18.7	0.56	2.6	5
LMC	SMP71	12710	0.067	0.036	1.6	22.2	8.3	4.73	5

TABLE 11—*Continued*

Galaxy	PN ID	T_e	He^0/H	He^+/H	$10^5 \times \text{O}^+/\text{H}$	$10^5 \times \text{O}^{++}/\text{H}$	$10^6 \times \text{N}^+/\text{H}$	$10^5 \times \text{Ne}^{++}/\text{H}$	Ref ^a
LMC	SMP13	14620	0.053	0.038	1.28	11.7	1.28	2.86	5
LMC	SMP37	14117	0.049	0.038	1.89	14.4	14.4	2.48	5
LMC	SMP66	11893	0.073	0.02		23.8	0.205	3.78	5
LMC	SMP84	14117	0.085		0.378	7.7		1.38	5
LMC	SMP101	15035	0.036	0.064	0.679	10.5	0.994	3.15	5
LMC	SMP3	13921	0.066		0.433	4.84	0.904	0.791	5
LMC	SMP97	14620	0.03	0.057	0.262	10.9	0.495	1.61	5
LMC	SMP85	11128	0.081		1.39	8.38	6.57	1.17	5
LMC	SMP8	11128	0.151		0.317	12.5	2.96	2.26	5
LMC	SMP87	25954	0.061	0.077	0.926	3.13	28.8	1.33	5
LMC	SMP36	14266	0.09	0.032		17.6	2.5	4.36	5
LMC	SMP51	12060	0.097		0.906	18.7	1.74	2.17	5
LMC	SMP45	15790	0.064	0.017	1.02	8.25	5.12	2.13	5
LMC	SMP10	17477	0.053	0.0043	0.674	5.33	4.71	1.77	5
LMC	SMP7	19548	0.034	0.069	1.1	5.54	20.5	1.01	5
LMC	SMP77	11324	0.118		2.88	7.25	4.1	0.946	5
LMC	SMP41	15354	0.036	0.05	0.872	9.13	9.23	2.2	5
LMC	SMP42	14878	0.082	0.007	0.111	9.89	0.907	1.63	5
LMC	SMP67	12145	0.094		4.12	5.18	28.6	1.15	5
LMC	SMP40	14518	0.042	0.051	2.66	9.68	11.4	3.12	5
LMC	SMP16	22802	0.058	0.065	0.951	3.28	19.1	1.24	5
LMC	SMP102	16410	0.033	0.063	0.131	5.75		0.92	5
LMC	SMP5	12935	0.062		4.07	4.2	1.37	0.238	5
LMC	SMP96	22962	0.097	0.081	0.634	2.69	22.5	1.13	5
LMC	SMP4	13680	0.037	0.032	0.184	13.3		3.08	5
LMC	SMP60	16238		0.085	0.274	7.19	1	1.81	5
LMC	SMP46	14826	0.053	0.028	2.65	9.94	16.6	2.49	5
LMC	SMP69	15516	0.037	0.065	1.52	7.65	44.9	2.31	5
LMC	SMP95	13395		0.025	5.74	13.2	19.8	4.15	5
LMC	SMP9	14467	0.056	0.034	4.38	8.45	15.8	3.11	5
LMC	SMP44	20386		0.055	1.11	3.95	24.8	1.42	5
LMC	SMP18	16641	0.081			6.23		1.2	5
LMC	SMP54	20673	0.044	0.078	1.19	3.53	32.1	1.42	5
LMC	SMP55	12800	0.071	0.0011	1.88	2.4	7.21		5
LMC	MG29	15141		0.058	2.12	8.82	9.72	2.32	5
LMC	SMP15	13727	0.105	0.026	1.57	12.8	2.81	3.48	5
LMC	SMP20	19075	0.056	0.059	0.886	3.88	23.6	1.55	5
LMC	SMP65	10596	0.114		0.768	21		2.78	5
LMC	SMP56	13025			2.53	3.95	1.45	0.204	5
LMC	SMP88	29958	0.033	0.085	0.143	0.671	2.16	0.236	5
LMC	SMP72	19209		0.068	0.26	4.59	0.829	0.711	5
LMC	SMP93	13584	0.061	0.047	5.74	6.24	142.1	3.35	5
LMC	MG83	27257		0.155	1.88	4.89	22.8	1.01	5
LMC	SMP2	12018	0.092		4.25	4.84	4.67		5
LMC	SMP24	12666		0.066	4.46	16.3	9.79	5.7	5

TABLE 11—*Continued*

Galaxy	PN ID	T_e	He ^o /H	He ⁺ /H	10 ⁵ × O ⁺ /H	10 ⁵ × O ⁺⁺ /H	10 ⁶ × N ⁺ /H	10 ⁵ × Ne ⁺⁺ /H	Ref ^a
LMC	MG45	15408	0.072	0.015	0.15	12.7	2.63	3.4	5
LMC	SMP14	20819	0.05	0.087	1.26	3.53	31.8	1.8	5
LMC	SMP31	12145	0.036		0.531	0.698	6.7	0.0117	5
LMC	MG46	17538		0.065	1.1	4.14	24.1	1.67	5
LMC	J21	20103		0.072		6.63		1.08	5
LMC	J24	18744		0.019	1.73	2.88	54.5	1.29	5
LMC	MG44	16467		0.065		5.78		1.05	5
LMC	J10	20891		0.072	0.193	2.41	2.16	0.645	5
M31 bulge	PN027	16013	0.102	0.0061	0.13	14.7	0.898	4.46	4,6
M31 bulge	PN029	10707	0.082	0.016	0.972	49.4	5.79	12	4,6,7
M31 bulge	PN001	10089		0.012	1.77	61.7	14.1	15.6	4,7
M31 bulge	PN023	13071	0.096	0.012	0.387	20.6		5.19	4,7
M31 bulge	PN056	15516		0.016	0.387	12.3		0.636	6
M31 bulge	PN181	29335		0.058	0.191	3.06		0.557	6
M31 bulge	PN033	12666	0.052	0.0034		19		4.37	4
M31 bulge	PN075	13286	0.483		1.25	19.1	6.32	3.19	4
M31 bulge	PN125	13286	0.102		0.534	12.3	4.42	2.14	4
M31 bulge	PN177	8926	0.13		6.55	23.6	35.4	7.44	4
M31 bulge	PN179	13286	0.102			10.5	5.52	2.88	4
M31 bulge	PN455	13286				14		0.857	4
M31 bulge	PN470	13286	0.826		11.74	10.3	27.5		4
M31 bulge	PN478	22643	0.083		0.41	1.77	1.88	0.35	4
M31 bulge	PN172	13071 ⁺²⁶⁰⁹ ₋₁₉₀₅	0.108 ^{+0.014} _{-0.017}	0.005 ^{+0.0007} _{-0.0006}	0.484 ^{+0.839} _{-0.302}	27.6 ^{+17.6} _{-10.9}		5.45 ^{+9.82} _{-3.49}	7
M31 bulge	PN031	10670 ⁺¹⁵⁶⁰ ₋₁₂₉₆		0.0053 ^{+0.0007} _{-0.0006}	1.08 ^{+1.63} _{-0.63}	63.1 ⁺³⁸ _{-22.9}		14.5 ^{+21.8} _{-8.5}	7
M31 bulge	PN080	< 9674		0.0064 ^{+0.0009} _{-0.0008}	2.78 ^{+4.51} _{-1.76}	71 ^{+23.1} _{-18.7}		12.9 ^{+15.6} _{-7.1}	7
M31 bulge	PN030	< 9276		0.019 ^{+0.007} _{-0.005}	7.35 ^{+11.82} _{-4.58}	93.2 ^{+30.8} _{-24.9}		15.7 ^{+19.6} _{-8.7}	7
M31 bulge	PN028	< 8619		0.0082 ^{+0.0018} _{-0.0013}	4.08 ^{+8.11} _{-2.68}	128 ^{+62.6} _{-44.4}		19.1 ^{+41.2} _{-13.1}	7
M31 bulge	PN012	13071 ⁺⁵⁶⁰⁷ ₋₃₁₉₂	0.082 ^{+0.007} _{-0.021}	0.018 ^{+0.009} _{-0.009}	1.34 ^{+1.11} _{-0.531}	26.5 ^{+16.1} _{-10.5}		6.6 ^{+36.37} _{-5.52}	7
M31 bulge	PN010	< 13584	0.164 ^{+0.04} _{-0.056}	0.012 ^{+0.004} _{-0.003}	0.376 ^{+1.609} _{-0.304}	16.1 ^{+13.6} _{-8.3}		2.53 ^{+10.93} _{-2.07}	7
M31 bulge	PN003	< 10231	0.253 ^{+0.027} _{-0.035}	0.0095 ^{+0.0021} _{-0.0017}	0.812 ^{+1.552} _{-0.531}	64.1 ^{+34.6} _{-23.5}		10 ^{+19.3} _{-6.6}	7
M31 bulge	PN038	< 10559		0.0064 ^{+0.0017} _{-0.0008}	0.818 ^{+1.744} _{-0.593}	35.7 ^{+13.1} _{-10.3}		5.42 ^{+7.67} _{-3.22}	7
M31 bulge	PN036	14518 ⁺³⁵⁸¹ ₋₂₅₄₂	0.063 ^{+0.006} _{-0.009}	0.006 ^{+0.0009} _{-0.0008}	0.345 ^{+0.676} _{-0.223}	13.1 ^{+9.9} _{-5.6}		3.56 ^{+7.22} _{-2.35}	7
M31 bulge	PN053	10089 ⁺¹⁶³⁸ ₋₁₄₄₀	0.201 ^{+0.009} _{-0.015}	0.0042 ^{+0.0005} _{-0.0005}	1.47 ^{+3.95} _{-1.05}	66.4 ^{+52.3} _{-26.5}		11.4 ^{+21.5} ₋₇	7
M31 bulge	PN052	< 11206	0.046 ^{+0.025} _{-0.019}	0.018 ^{+0.012} _{-0.008}	1.79 ^{+4.72} _{-1.3}	32.8 ^{+19.2} ₋₁₄		4.13 ^{+11.69} _{-3.11}	7
M31 bulge	PN042	12359 ⁺¹⁸⁰⁷ ₋₁₄₂₅	0.083 ^{+0.006} _{-0.008}	0.0052 ^{+0.0006} _{-0.0006}	0.402 ^{+0.514} _{-0.222}	37.5 ^{+18.7} _{-12.6}		5.87 ^{+7.43} _{-3.25}	7
M31 bulge	PN045	15035 ⁺²¹⁹⁹ ₋₁₆₈₇	0.106 ^{+0.01} _{-0.011}	0.0037 ^{+0.0003} _{-0.0003}	0.277 ^{+0.42} _{-0.177}	14.5 ^{+5.7} _{-4.2}		3.11 ^{+2.98} _{-1.53}	7
M31 bulge	PN043	< 11404	0.122 ^{+0.009} _{-0.016}	0.006 ^{+0.0009} _{-0.0007}	0.841 ^{+1.079} _{-0.467}	32.4 ^{+11.5} _{-9.1}		6.71 ^{+9.2} _{-3.89}	7
M31 bulge	PN048	9810 ⁺¹¹⁶² ₋₁₀₃₉	0.201 ^{+0.008} _{-0.011}	0.0033 ^{+0.0021} _{-0.0018}	0.67 ^{+0.803} _{-0.347}	77.2 ^{+41.3} _{-25.2}		18.2 ^{+21.5} _{-9.3}	7
M31 bulge	PN095	< 9276	0.132 ^{+0.008} _{-0.009}	0.0025 ^{+0.0002} _{-0.0002}	1.34 ^{+1.33} _{-0.72}	45.1 ^{+7.4} _{-6.2}		8.89 ^{+4.8} _{-3.05}	7
M31 bulge	PN047	9540 ⁺¹⁶⁶⁶ ₋₁₅₈₇	0.148 ^{+0.01} _{-0.013}	0.0035 ^{+0.0004} _{-0.0004}	1.17 ^{+4.35} _{-0.91}	59.2 ^{+61.5} _{-25.2}		8.31 ^{+19.47} _{-5.24}	7
M31 bulge	PN408	< 11209		0.027 ^{+0.012} _{-0.007}		34 ^{+66.2} _{-19.9}			7
M31 bulge	PN093	< 10935	0.165 ^{+0.024} _{-0.036}	0.013 ^{+0.006} _{-0.004}	1.68 ^{+4.15} _{-1.21}	51.6 ^{+21.7} _{-17.2}		7.82 ^{+13.78} _{-4.97}	7
M31 bulge	PN092	11810 ⁺²⁰⁶³ ₋₁₆₈₅	0.126 ^{+0.02} _{-0.02}	0.005 ^{+0.0006} _{-0.0005}	1.71 ^{+3.82} _{-1.16}	34.7 ^{+23.2} _{-13.2}		7.05 ^{+12.24} _{-4.32}	7
M31 bulge	PN097	9440 ⁺¹⁰⁸² ₋₁₂₀₄	0.157 ^{+0.015} _{-0.015}	0.0035 ^{+0.0002} _{-0.0002}	1.12 ^{+1.26} _{-0.48}	73.7 ^{+55.7} _{-25.2}	8.3 ^{+4.52} _{-2.31}	11 ^{+13.4} _{-5.1}	7
M31 bulge	PN091	12710 ⁺²⁹⁷⁰ ₋₂₁₈₉		0.0065 ^{+0.001} _{-0.0009}	0.555 ^{+1.267} _{-0.372}	23.5 ^{+19.7} _{-10.4}		2.81 ^{+6.84} _{-1.95}	7

TABLE 11—*Continued*

Galaxy	PN ID	T_e	He ^o /H	He ⁺ /H	$10^5 \times \text{O}^+/\text{H}$	$10^5 \times \text{O}^{++}/\text{H}$	$10^6 \times \text{N}^+/\text{H}$	$10^5 \times \text{Ne}^{++}/\text{H}$	Ref ^a
M31 bulge	PN387	10522 ⁺¹⁴⁵⁵ ₋₁₂₄₅	0.12 ^{+0.01} _{-0.014}	0.013 ^{+0.004} _{-0.003}	4.76 ^{+7.88} _{-2.9}	46.7 ^{+27.5} _{-16.4}		9.45 ⁺¹³ _{-5.29}	7
M31 bulge	PN380	14068 ⁺¹⁴⁴⁸ ₋₁₃₅₈	0.115 ^{+0.012} _{-0.012}	0.0046 ^{+0.0003} _{-0.0003}	0.366 ^{+0.211} _{-0.124}	22.8 ^{+9.3} _{-6.1}	1.47 ^{+0.51} _{-0.37}	3.6 ^{+2.44} _{-1.39}	7
M31 disk	FJCHP51	11686	0.093	0.037	1.3	31.8	19	6.79	4
M31 disk	FJCHP57	10973	0.108		1.35	17.5	4.83	0.227	4
M31 disk	FJCHP58	11011	0.081	0.0074		25.6		4.33	4
M31 disk	PN290	10670	0.142	0.0046	3.23	26.1	9.65	4.62	9
M31 disk	PN363	11284	0.144		4.47	34	11.9	9.68	9
M31 disk	PN372	16525			0.3	9.24	2.18	2.76	9
M32	PN24	18354 ⁺⁴⁸⁵⁰ ₋₃₄₇₆	0.124 ^{+0.102} _{-0.086}	0.035 ^{+0.024} _{-0.015}	0.794 ^{+1.763} _{-0.527}	10.8 ^{+10.7} _{-5.1}	14 ^{+6.8} _{-4.5}	2.16 ^{+4.31} _{-1.39}	7
M32	PN6	13117 ⁺³⁷⁰⁰ ₋₃₂₃₈	0.19 ^{+0.071} _{-0.056}	0.03 ^{+0.024} _{-0.015}	0.402 ^{+2.83} _{-0.365}	25.8 ^{+50.5} _{-14.2}	4.27 ^{+5.14} _{-1.99}	5.58 ^{+24.02} _{-4.14}	7
M32	PN25	< 18941	0.204 ^{+0.061} _{-0.051}	0.035 ^{+0.033} _{-0.012}		9.73 ^{+13.04} _{-5.48}	7.84 ^{+2.77} _{-2.86}	2.29 ^{+9.69} _{-1.8}	7
NGC 147	PN02	15354 ⁺³⁷⁸⁷ ₋₂₆₈₈	0.076 ^{+0.024} _{-0.022}	0.0031 ^{+0.0021} _{-0.0013}	0.0913 ^{+0.2438} _{-0.0666}	8.5 ^{+9.15} _{-4.27}	1.21 ^{+0.74} _{-0.49}	0.797 ^{+1.736} _{-0.539}	10
NGC 147	PN03	16013 ⁺²⁶⁶⁶ ₋₂₁₄₀	0.038 ^{+0.01} _{-0.009}	0.012 ^{+0.005} _{-0.004}		6.35 ^{+4.3} _{-2.47}	0.0691 ^{+0.0389} _{-0.0274}	0.193 ^{+0.267} _{-0.112}	10
NGC 147	PN04	8895 ⁺⁸⁸¹ ₋₈₅₈	0.147 ^{+0.022} _{-0.021}	0.0014 ^{+0.0006} _{-0.0004}	2.53 ^{+3.61} _{-1.41}	18.9 ^{+13.3} _{-7.1}	12.4 ^{+5.1} _{-3.3}	1.87 ^{+2.55} _{-1.03}	10
NGC 147	PN07	11050 ⁺¹⁴⁴⁰ ₋₁₂₄₀	0.134 ^{+0.023} _{-0.023}	0.0033 ^{+0.0016} _{-0.0012}	0.175 ^{+0.29} _{-0.109}	19.4 ^{+13.6} _{-7.6}	0.199 ^{+0.116} _{-0.079}		10
NGC 147	PN06	< 14569	0.035 ^{+0.012} _{-0.011}	0.005 ^{+0.0029} _{-0.0021}	0.439 ^{+0.955} _{-0.292}	7.42 ^{+7.9} _{-3.57}	8.87 ^{+5.34} _{-3.22}		10
NGC 147	PN01	13921 ⁺²³⁷⁴ ₋₁₉₈₇	0.089 ^{+0.024} _{-0.022}	0.0086 ^{+0.0039} _{-0.0029}	0.0778 ^{+0.1416} _{-0.0494}	9 ^{+7.18} _{-3.74}	0.528 ^{+0.306} _{-0.199}		10
Sagittarius	He 2-436	14417	0.115	0.0006	0.145	9.18	0.909	1.6	11
Sagittarius	Wray 16-42	12490	0.106	0.0096	0.603	18.6	1.94	3.26	11
Sagittarius	StWr 2-21	11484 ⁺⁴⁰ ₋₄₀	0.072 ^{+0.001} _{-0.001}	0.035 ⁺⁰ ₋₀	1.05 ^{+0.06} _{-0.05}	22.6 ^{+0.3} _{-0.3}	1.62 ^{+0.03} _{-0.03}	4.54 ^{+0.07} _{-0.07}	12
Fornax	PN01	10195 ⁺³⁶³ ₋₃₁₆	0.101 ^{+0.007} _{-0.006}	0.0002 ^{+0.0001} _{-0.0001}	1.92 ^{+1.61} _{-0.9}	17.6 ^{+3.2} _{-2.7}	1.03 ^{+0.14} _{-0.12}	2.51 ^{+0.75} _{-0.6}	13

^aReferences for line intensities: (1) van Zee et al. (2006); (2) Magrini et al. (2005); (3) Kniazev et al. (2005); (4) Jacoby & Ciardullo (1999); (5) a compilation of Aller et al. (1987), Barlow (1987), Monk et al. (1987), Wood et al. (1987), Dopita et al. (1988), Meatheringham et al. (1988), Henry et al. (1989), Meatheringham et al. (1988), Meatheringham & Dopita (1991a), Meatheringham & Dopita (1991b), Dopita & Meatheringham (1991), Vassiliadis et al. (1992), Jacoby & Kaler (1993), Leisy & Dennefeld (1996); see Richer (1993), Richer & McCall (1995), and Stasińska et al. (1998) for more details; (6) Roth et al. (2004); (7) Richer et al. (1999); (8) Richer & McCall (2007); (9) Jacoby & Ford (1986); (10) Gonçalves et al. (2006); (11) Dudziak et al. (2000); (12) Zijlstra et al. (2006); (13) Kniazev et al. (2006)

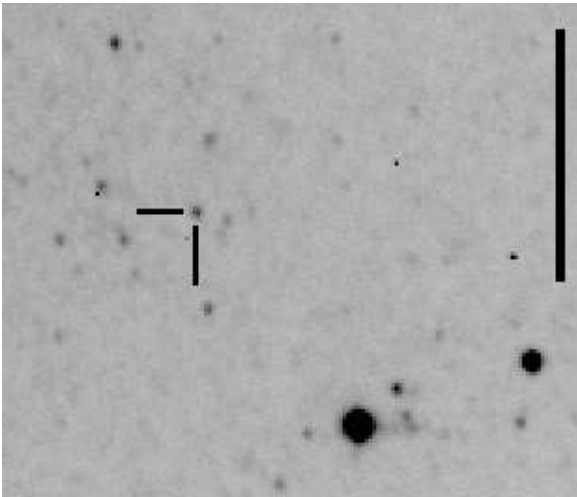


Fig. 1.— This is a finder chart ($[\text{O III}]\lambda 5007$) for PN #3273 from the list of Merrett et al (2006), in the field of M32. North is up and east is to the left. The vertical bar at right is $30''$ long.

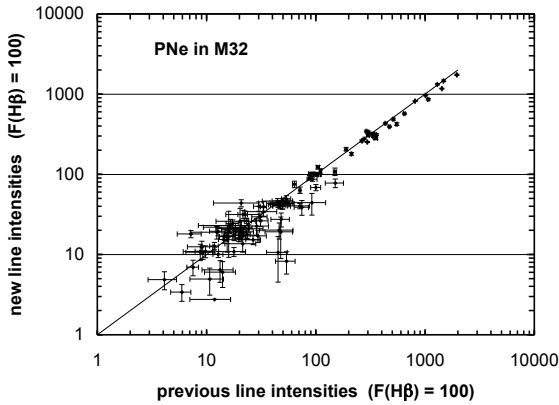


Fig. 2.— Line intensities presented here for planetary nebulae in M32 are compared with those presented in Richer et al. (1999). None of the line intensities are corrected for reddening. The diagonal line indicates perfect agreement. Generally, the agreement is reasonable. Lines stronger than $H\beta$ have relative uncertainties of about 10% while those whose intensities are of order $0.1I(H\beta)$ have relative uncertainties of order 100%.

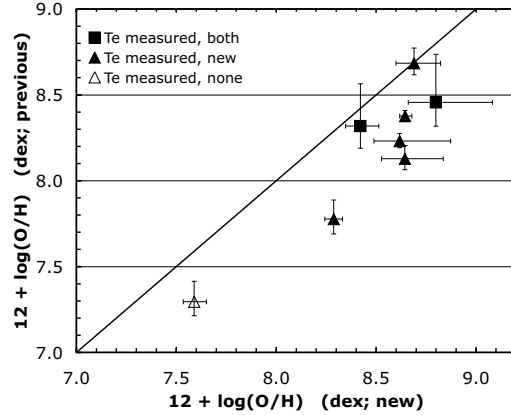


Fig. 3.— Oxygen abundances presented here for planetary nebulae in M32 are compared with those presented in Richer et al. (1999). The symbols differentiate objects with measured temperatures from those with only upper limits to the temperature in the previous or both studies. The diagonal line indicates perfect agreement, expected only for objects with temperatures measured in both studies. The electron temperatures or limits found here are lower than the upper limits formerly available, so our oxygen abundances are larger.

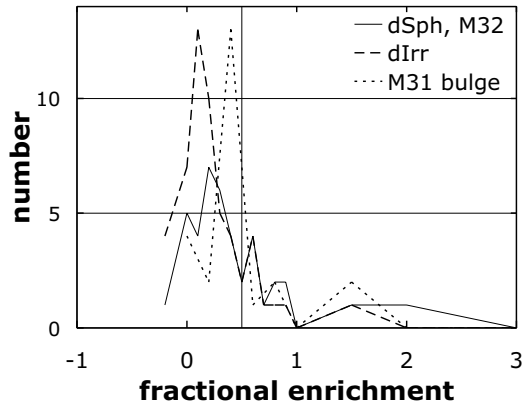


Fig. 9.— These histogram present distributions of the helium enrichment in bright planetary nebulae. Enrichment is defined as the increase relative to the relation expected in the interstellar medium in dwarf star-forming galaxies (Olive et al. 1997). The vertical line corresponds to an enrichment by 50% with respect to the supposed helium abundance in the progenitor.

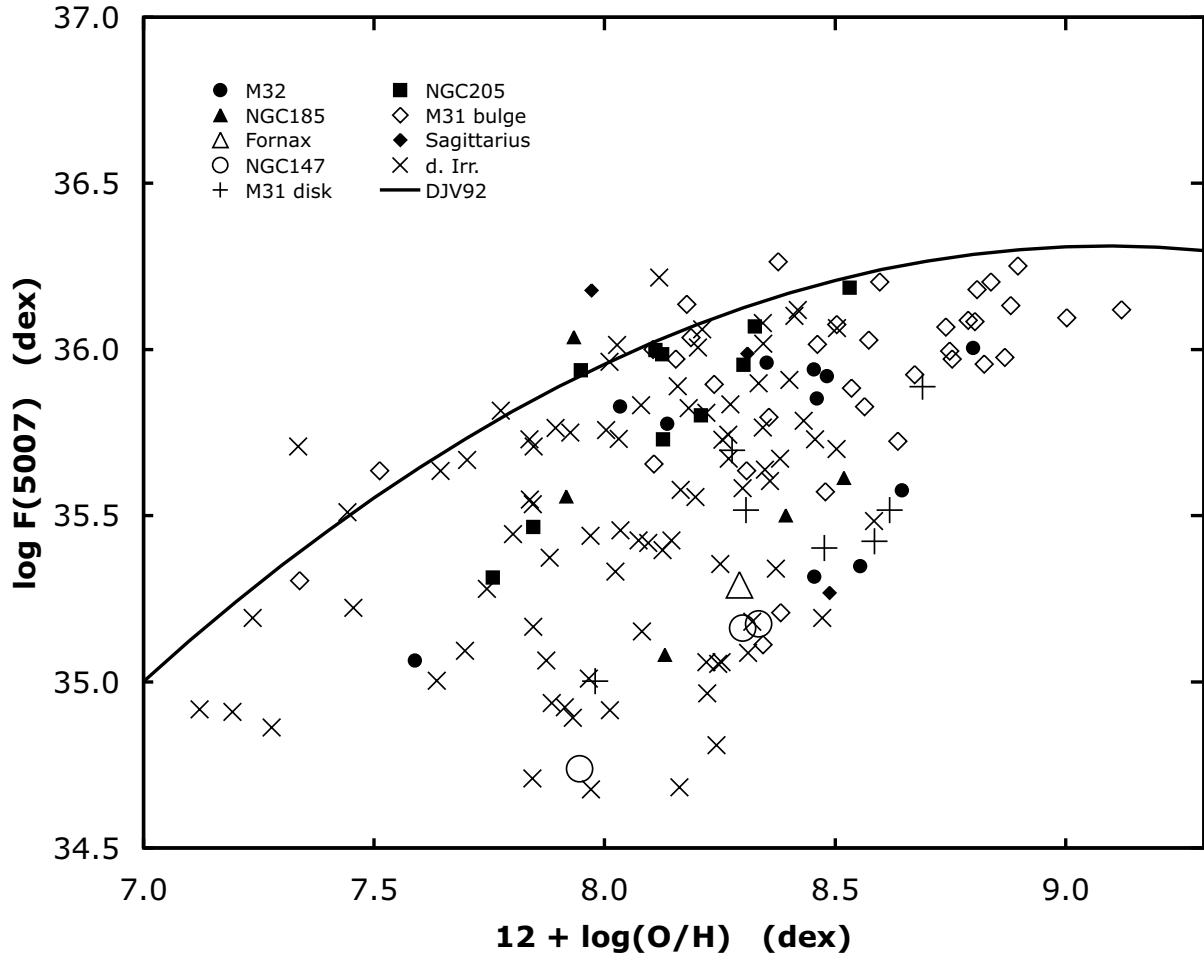


Fig. 4.— We plot the absolute luminosity in $[\text{O III}]\lambda 5007$ as a function of oxygen abundance for all of the bright extragalactic planetary nebulae considered here. The solid line is the relation found theoretically by Dopita et al. (1992). Below $12 + \log(\text{O}/\text{H}) \sim 7.9$ dex, the $[\text{O III}]\lambda 5007$ luminosity appears to depend upon the oxygen abundance, but there is no obvious dependence at higher abundances. Note that the $[\text{O III}]\lambda 5007$ luminosities are not corrected for reddening and are based upon the distances in Richer & McCall (1995), except for Leo A, whose distance is adopted from Lee et al. (2003).

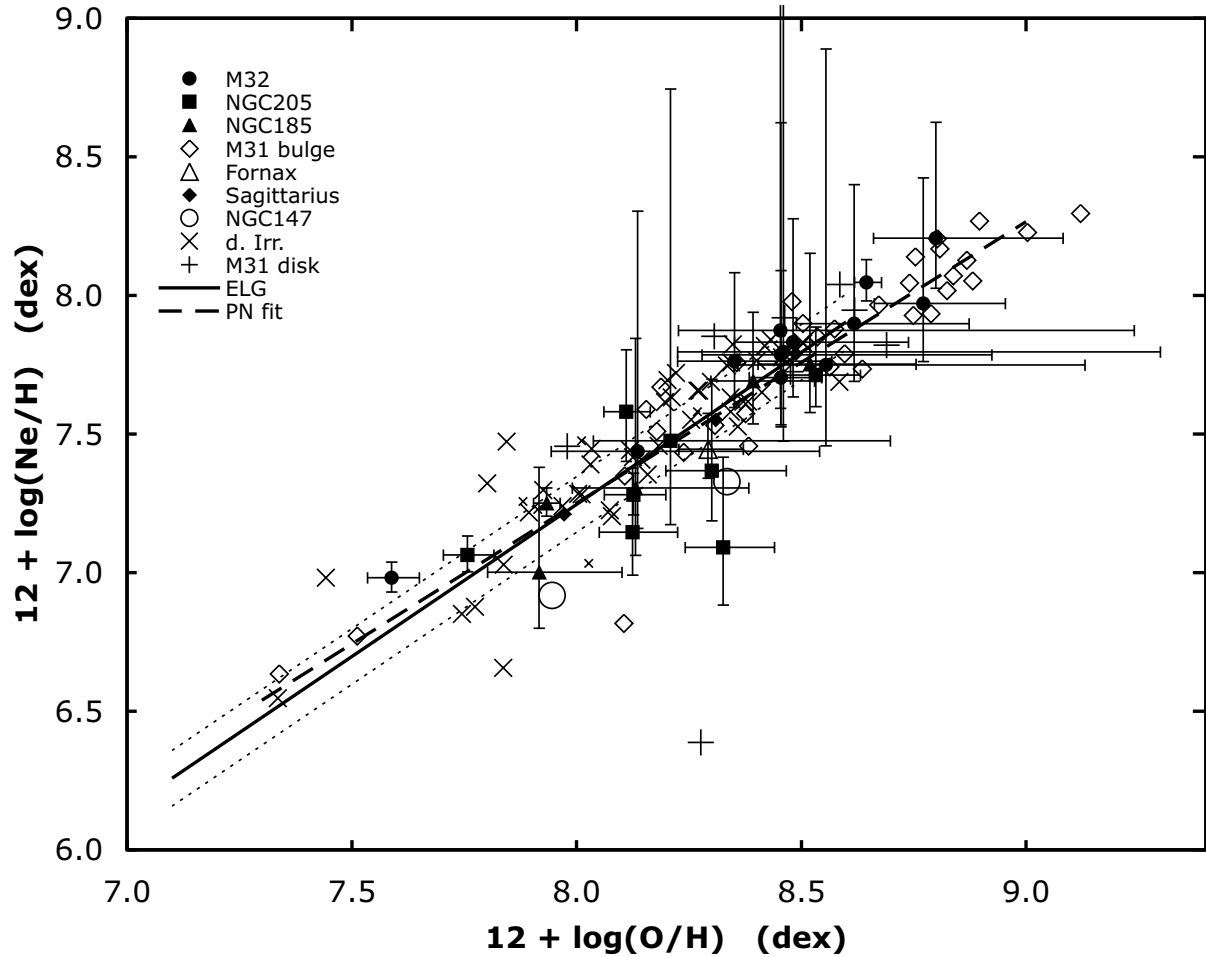


Fig. 5.— Neon abundances are plotted as a function of oxygen abundances for planetary nebulae in M32, NGC 185, and NGC 205. The data for other galaxies are drawn from the literature. The dashed line is a fit to these abundances in planetary nebulae in galaxies without star formation. The solid line shows the relation between oxygen and neon abundances in emission-line galaxies (ELGs) from Izotov et al. (2006), with the dotted lines denoting the scatter about their relation. Clearly, the data for bright planetary nebulae are not obviously offset from that for emission-line galaxies. In this and following diagrams, error bars are only shown for the planetary nebulae in M32, NGC 185, and NGC 205 to help improve clarity. In general (here and in the following plots), the uncertainties are similar for the LMC, SMC, NGC 147, and NGC 6822, significantly lower for Sex A, Sex B, Leo A, Fornax, and Sagittarius, and slightly larger for the planetary nebulae in the bulge and disk of M31. For reference, the median uncertainty for the oxygen abundances in NGC 185, NGC 205, and M32 is approximately 0.2 dex.

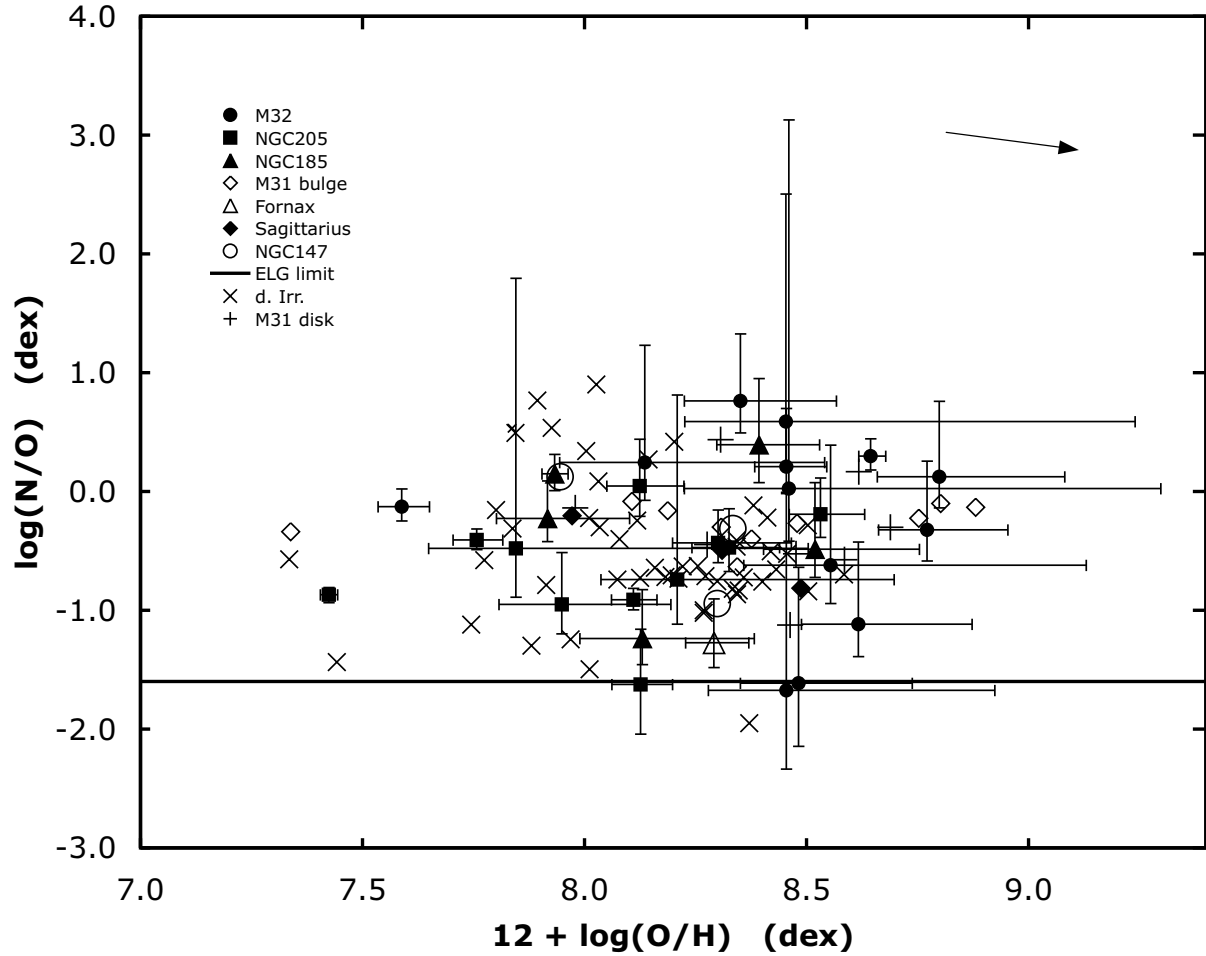


Fig. 6.— The N/O ratio is plotted as a function of oxygen abundance for the bright planetary nebulae in M32, NGC 185, and NGC 205 as well as for their counterparts in other galaxies drawn from the literature. For clarity, error bars are only drawn for the data presented in this paper (see Fig. 5). The arrow indicates the change in position of a point if the temperature decreases from $1.5 \times 10^4\text{K}$ to 10^4K , assuming $12 + \log(\text{O}/\text{H}) = 8.0$ dex. The horizontal line denotes the lower limit to the N/O ratio found in emission-line galaxies (Izotov et al. 2006). It is somewhat surprising that the N/O ratio in bright planetary nebulae covers the same range in galaxies with and without ongoing star formation.

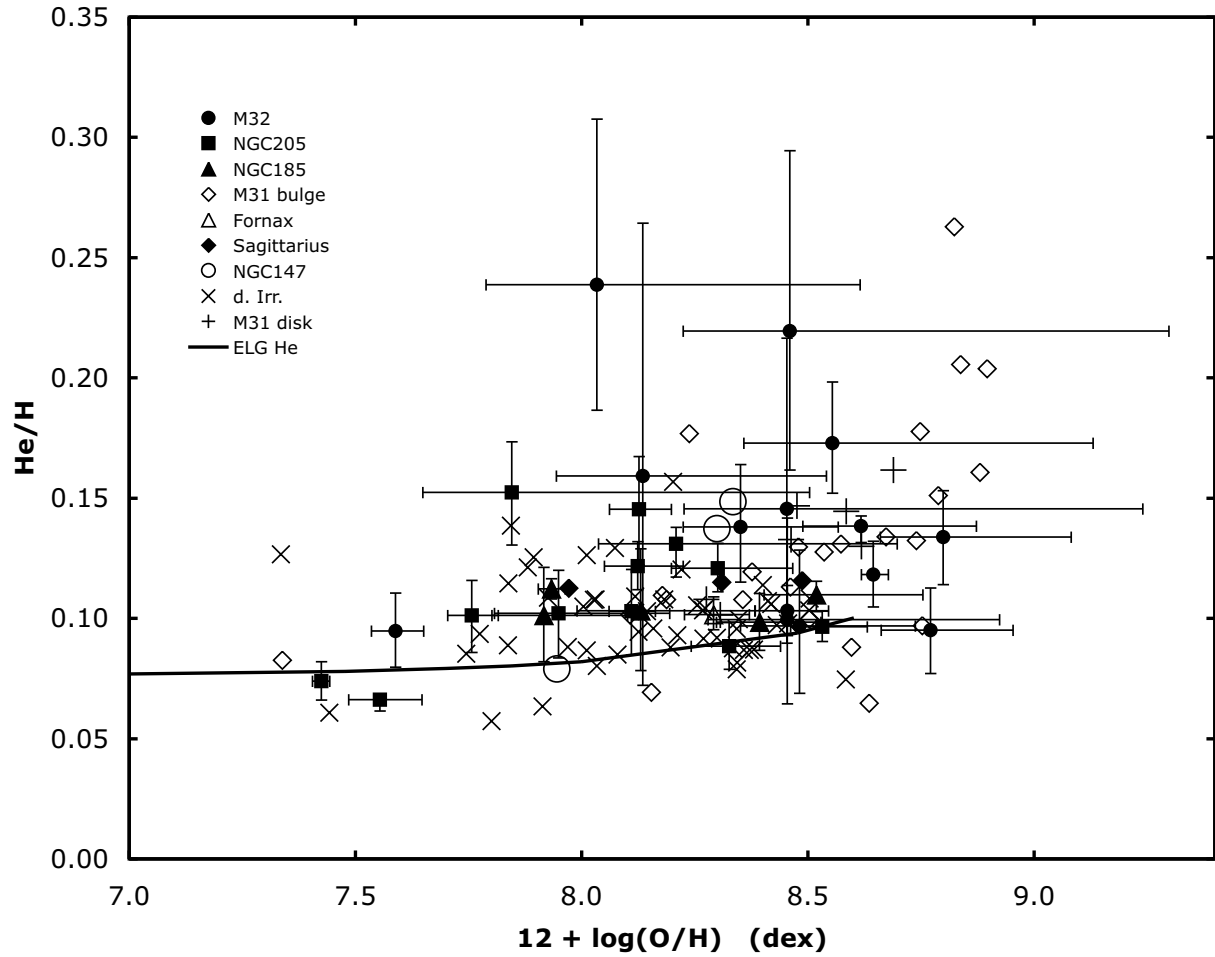


Fig. 7.— The helium abundance is plotted as a function of the oxygen abundance for the bright planetary nebulae in M32, NGC 185, and NGC 205 as well as for their counterparts in other galaxies drawn from the literature. For clarity, error bars are only drawn for the data presented in this paper (see Fig. 5). The line shows the relation between helium and oxygen abundances in H II regions in emission-line galaxies from Olive et al. (1997, sample B).

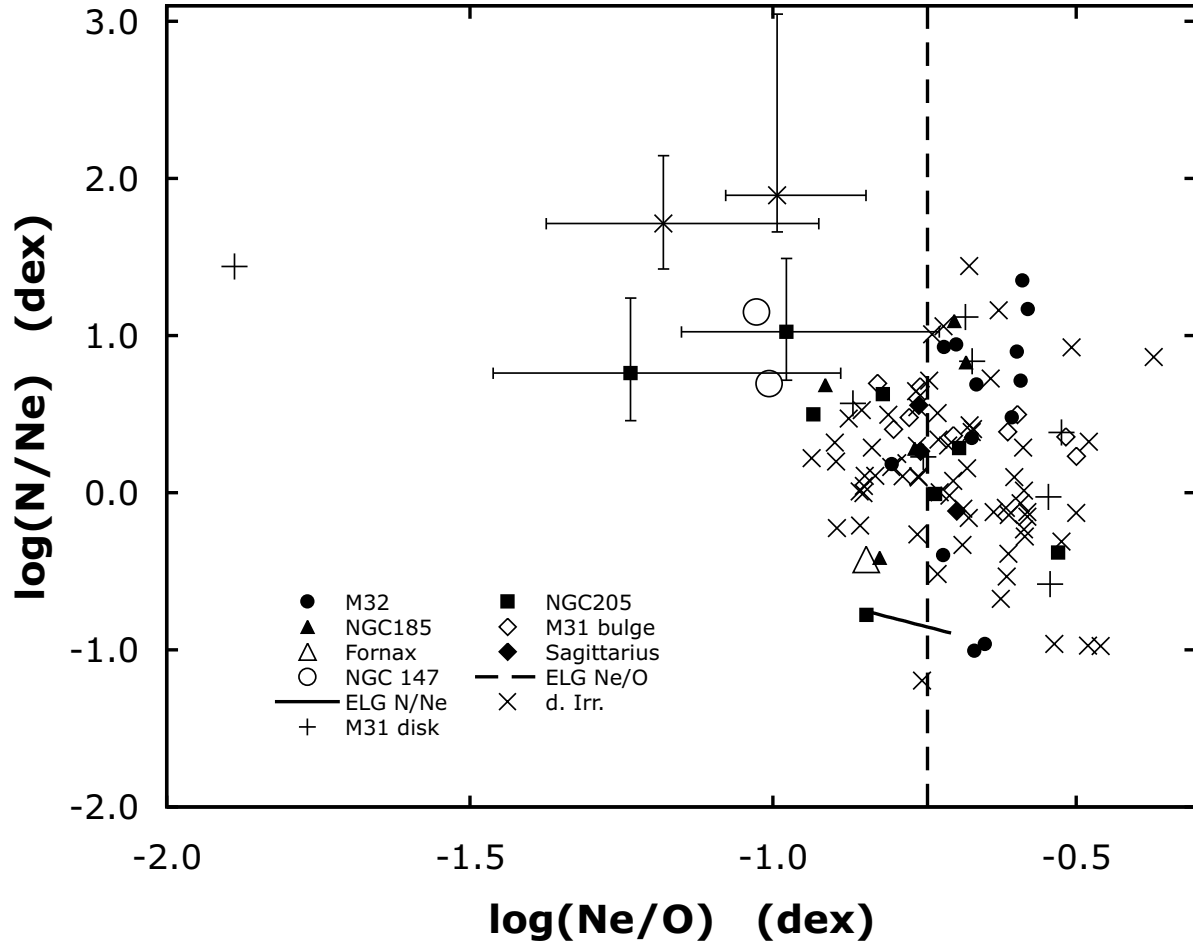


Fig. 8.— The N/Ne ratio is plotted as a function of the Ne/O ratio for the bright planetary nebulae in M32, NGC 185, and NGC 205 as well as for their counterparts in other galaxies drawn from the literature. For clarity, error bars are only drawn for the objects that appear to have dredged up oxygen (if these errors are known). The vertical dashed line shows the Ne/O ratio found in emission-line galaxies at an oxygen abundance of $12 + \log(\text{O}/\text{H}) = 8.0$ dex while the short solid line shows the relation between N/Ne and Ne/O as the oxygen abundance varies over the interval $7.0 \text{ dex} < 12 + \log(\text{O}/\text{H}) < 8.5$ dex, assuming the limiting value of N/O (Izotov et al. 2006).